Estimating Forest metrics in interior Alaska with terrestrial Lidar.

Rachel Deininger

A thesis

submitted in partial fulfillment of the

requirements for the degree of

Master of Science

University of Washington

2025

Committee:

L. Monika Moskal

Hans-Erik Andersen

Jonathan L Batchelor

Program Authorized to Offer Degree:

School of Environmental and Forest Sciences

University of Washington

Abstract

Estimating Forest metrics in interior Alaska with terrestrial Lidar.

Rachel Deininger

Chair of Supervisory Committee:
L. Monika Moskal
School of Environmental and Forest Sciences

This thesis contains multiple research documents, including a report for the Forest Service, a detailed field guide, a metadata document, and a research proposal.

Boreal forests make up a third of global forested area and play a vital role in global carbon storage, but their vulnerability to climate change necessitates improved methods for monitoring. We need accurate models of forest structure to understand how boreal forests will respond to climate change. Lidar remote sensing shows potential to fulfil this need by providing fine-scale models of individual trees. study assesses the application of Terrestrial Laser Scanning (TLS) to estimate Above Ground Biomass (AGB) in Alaska's boreal forests, focusing on its performance compared to traditional Forest Inventory and Analysis (FIA) methods. TLS, using the FARO Focus S360 scanner, detected significantly more trees than FIA, especially smaller trees that FIA does not measure due to its diameter threshold. These differences in stem count are most pronounced in black spruce and mixed forests. Trees from the segmented TLS point clouds were matched with FIA manually measured trees. The matched trees were used to train a Random Forest model to predict tree species. With predicted species for all TLS detected trees, a species specific allometric equation to predict biomass was employed on an individual tree level. Statistical tests, including Kruskal-Wallis and Dunn's post-hoc tests, revealed that forest type and

species composition significantly influenced errors in TLS-derived metrics, with deciduous forests showing the lowest variability in biomass estimates. Due to its ability to capture smaller trees, TLS identifies a greater amount of biomass, particularly in black spruce forests. The findings highlight TLS's potential to improve biomass estimates but also emphasize the need for careful calibration and species-specific adjustments. Future work should focus on integrating TLS with airborne and mobile Lidar technologies to scale forest structure assessments across broader landscapes.

The field guide in Appendix A. provides a framework for conducting terrestrial and mobile laser scans in forest inventory in Alaska’s boreal forests. By standardizing data collection and analysis protocols, this field guide aims to support the U.S. Forest Service's Forest Inventory and Analysis (FIA) program and advance the use of Lidar for assessing forest structure, carbon dynamics, and resilience in boreal ecosystems. The metadata document in Appendix B. provides detailed descriptions of data collected during field campaigns in Alaskan. These datasets are the product of this study, containing details of tree structural metrics such as diameter at breast height (DBH), height, projected area, and alpha volume, calculated from TLS, as well as derived attributes like biomass, proximity, and species predictions. The research proposal in Appendix C., funded by the Gloria Barron Wilderness Society Scholarship, addresses the need for monitoring forest state changes in Alaskan wilderness areas. The study plans to integrate aerial laser scanning (ALS) and mobile laser scanning (MLS), to develop a scalable method for quantifying forest structural complexity and monitoring ecological trajectories in boreal forests.

Table of Contents

List of Figures

List of Tables

1 Introduction

1.1 1.1 Boreal Forests

Boreal Forests cover 30% of Earth's forested area and account for 14.5% of the total land area on Earth (Liu et al. 2021). These forests are imperiled by warming, which is four times faster than the global average (Rantanen et al. 2021), resulting in 20% of the global/boreal permafrost being at risk of abrupt thawing (Nitze et al. 2018; Calvin et al. 2023). Permafrost thaw has the potential to release large quantities of organic carbon, causing further warming and disruption to the climate (Jones et al. 2023; Jorgenson et al. 2010). Although boreal forests exhibit resilience (defined as the capacity of a system to maintain functions, structures, and feedback in response to disturbances (Chapin et al. 2010; Albrich et al. 2020)) and are adapted to harsh conditions (Hessburg et al. 2019; Thompson 2009; Weldon and Grandin 2019), contemporary climate change far outpaces the variability experienced by boreal forests in the past (Calvin et al. 2023). Increasing temperatures and prolonged droughts increase tree stress, making them more susceptible to insect infestations and diseases. Additionally, higher temperatures can create a positive feedback loop in boreal regions. As soil temperatures rise, decomposition rates increase, releasing more carbon into the atmosphere, further accelerating climate change (Lim et al. 2019).

Boreal forests are also nitrogen-limited because of the temperature constraints that restrict nitrogen mineralization. However, higher temperatures may increase the decomposition of organic matter, releasing more bioavailable nitrogen, and potentially enhancing vegetation growth and carbon sequestration (Lim et al. 2019). Nevertheless, questions remain regarding whether this increased growth can persist long enough to offset carbon emissions resulting from accelerated soil decomposition and more frequent larger fires over extended periods.

1.2 1.2 FIA

The Forest Inventory and Analysis (FIA) program is a nationwide initiative led by the U.S. Forest Service to monitor the health, growth, and changes in forests across the country (Blehm, Ave, and Paul 2010). The FIA systematically collects data on forested lands with more than 10% canopy coverage, including those in interior Alaska. These data are essential for estimating forest area, classifying forest types, evaluating tree health, and monitoring changes over time. Due to interior Alaska's vast wilderness and remote areas, the FIA sampling intensity is lower than that in the contiguous U.S., with one plot measured every 30,000 acres (Schulz 2014). The size and remote nature of Alaska make field data collection more time-consuming and expensive. In 2014, Alaska FIA began to utilize remote sensing technologies, such as Lidar, hyperspectral, and thermal imaging, to supplement or enhance manual data collection.

This research aims to provide the U.S. Forest Service (USFS) and Forest Inventory Analysis (FIA) with enhanced AGB data, improving the accuracy of forest biomass estimates, which are essential for informing management strategies related to carbon management and climate adaptation. Integrating TLS data into existing FIA methodologies will strengthen the robustness of forest inventories and contribute to more informed resource management practices.

1.3 1.3 Remote Sensing and Lidar

Remote sensing technologies have been extensively used to study various ecological properties such as landscape features, vegetation stress, and biomass. Remote sensing offers a

fast, non-intrusive method for studying Earth's surface. It can be performed passively (e.g., optical) or actively (e.g., radar and lidar). Optical remote sensing has the highest volume of available data, especially from satellites such as NASA's Landsat program, which has provided consistent data since 1972 (Vorster et al. 2020).

Lidar (Light Detection and Ranging) is an active remote sensing technique that emits light in pulses to measure the distance between the scanner and an object (Bauwens et al. 2016). The scanner generates a point cloud representing the scanned area, with applications ranging from autonomous vehicles to mapping forest structure (Hyyppä et al. 2013). Among Lidar technologies, phase-shift and time-of-flight Lidar are the two primary approaches for measuring distances (Batchelor et al. 2023). Phase-shift Lidar emits a continuous modulated laser beam and calculates the distance by measuring the phase difference between the outgoing and returning light waves. This allows for fast, high-resolution scans at a close range, although it limits the effective range and prevents multiple returns from a single pulse. In contrast, time-of-flight lidar emits discrete pulses and measures the time taken by each pulse to return. This approach enables longer-range scanning with the capability of capturing multiple returns, making it ideal for capturing complex structures such as forest canopies. In forestry, lidar can be used to measure various metrics, including stem maps, canopy height, aboveground biomass (AGB), and diameter at breast height (DBH) (Heidenreich and Seidel 2022). It also enables monitoring of forest structural changes over time, which can indicate the effects of environmental stressors on forest vitality (Heidenreich and Seidel 2022). Forest structural diversity is an essential predictor of forest function, influencing factors such as microclimate, hydrology, and forest resilience (LaRue et al. 2020).

Although Lidar has limited spatial and temporal coverage, it is widely regarded as the most accurate remote sensing tool for estimating forest structure attributes, making it the preferred method for forest inventory assessments (Vorster et al. 2020; Hudak et al. 2020). Lidar scanners can be deployed on various platforms, including spaceborne, airborne, and terrestrial systems (Bauwens et al. 2016).

1.4 Terrestrial Laser Scanning (TLS) and Mobile Laser Scanning (MLS)

Terrestrial Laser Scanning (TLS) is a ground-based lidar system that collects high-resolution data from a stationary position, such as on a tripod or a vehicle-mounted scanner (Bauwens et al. 2016). While TLS provides detailed measurements of individual trees, it covers smaller areas than airborne laser scanning (ALS), which is typically mounted on aircraft and can cover large areas more rapidly. A study comparing ALS and TLS by LaRue et al. (2020) found strong agreement in several metrics, such as canopy height and leaf area, but noted challenges with TLS when measuring the top of the canopy due to occlusion from lower foliage. Single-scan TLS has been used in many studies for vegetation sampling by capturing detailed structural metrics, such as diameter at breast height (DBH), vegetation density, openness, and patchiness, allowing for fine-scale ecological assessments (Batchelor et al. 2022; Richardson and Moskal 2014). Although it offers powerful insights into vegetation structure with minimal setup, single-scan TLS can be limited by occlusions from nearby objects, which may obstruct parts of the scan and reduce data accuracy in more complex or dense vegetation environments. Collecting multiple scans from different positions with TLS can mitigate the effect of occlusion; however, it makes data collection and processing more time consuming (Hyyppä et al. 2013; Bauwens et al. 2016).

Mobile Laser Scanning (MLS) is a subset of TLS, utilizing handheld or vehicle-mounted devices that allow for greater mobility and efficiency in data collection. MLS systems are easier to deploy in remote or difficult terrain compared to tripod-mounted TLS devices (Bauwens et al. 2016). Although MLS systems may sacrifice some fine detail accuracy in comparison to multi-scan TLS, they have been found to offer faster acquisition times and improved tree detection rates, making them suitable for large-scale forest inventories in remote locations (Kükenbrink et al. 2022). Many MLS devices use a technique called Simultaneous Localization and Mapping (SLAM) which has become pivotal in forest mapping, particularly for addressing the challenges of scanning in GNSS-obstructed environments such as dense boreal forests (Shao et al. 2020). SLAM enables MLS systems to accurately map environments while simultaneously estimating their trajectories, mitigating issues like GNSS drift and occlusions through feature-based optimization. Graph-based SLAM, as demonstrated in a study using an ATV-mounted MLS system, leverages sparse environmental features, such as tree stems, to construct pose graphs and iteratively optimize the trajectory. This approach significantly improved positional accuracy, reducing errors from 0.7 meters to 1 centimeter and enhancing the reliability of 3D terrain and tree maps for forestry applications (Kukko et al. 2017) .

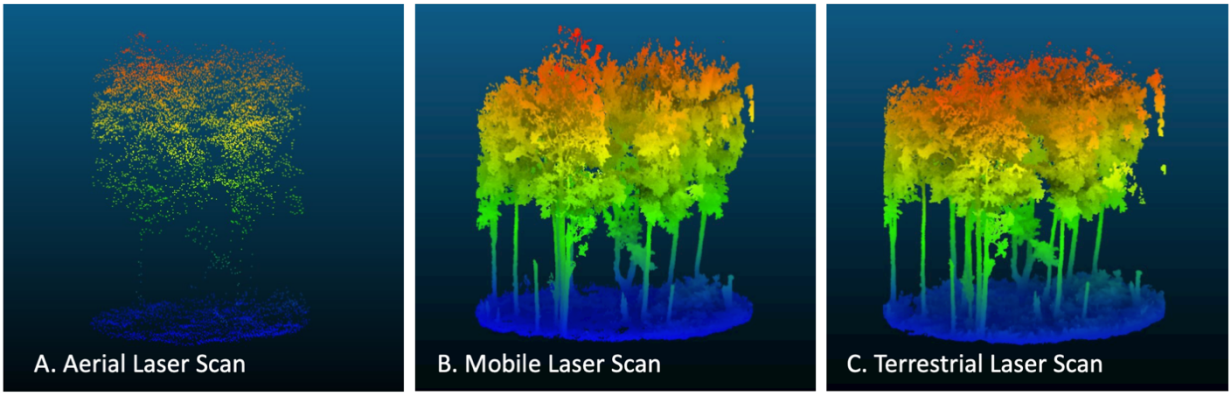

Figure 1: Example scans from A. aerial, B. terrestrial, and C. mobile laser scanner from the same region. Figure illustrates the visible differences in point density between Lidar types.

1.5 Lidar Metrics and Climate Change

Any robust forest inventory approach must consider the cost-effectiveness of the tools used in the data analysis. In the geospatial field, open-source software has become an attractive and cost-effective option. For instance, NASA's research efforts increasingly rely on open-source infrastructure (Webb and Solar, n.d.). One critical aspect of forest inventory is segmentation, which is the process of dividing lidar point clouds into meaningful regions, such as individual trees or tree clusters. Segmentation is essential for extracting key structural attributes such as tree height, crown size, and biomass estimates. Open-source software packages for R, such as Spanner, lidR, and ITSME, offer powerful tools for the segmentation of Lidar data. Spanner is a TLS and MLS specific packages that is used to segment point clouds into individual trees (Donager, Sánchez Meador, and Blackburn 2021; Sánchez Meador, Donager, and Cannon 2022). The package lidR is designed to work with ALS point clouds and has a wide variety of applications (Roussel et al. 2020). ITSME is used on individual tree point clouds or quantitative structural models of individual trees to calculate structural metrics (Terryn et al. 2023). These packages

provide an accessible and low-cost solution for forest structure analyses. Terryn et al. (2020), used forest structural metrics calculates from TLS to predict tree species.

As forests continue to face the challenges of anthropogenic climate change, traditional forest management must adapt to increased variability in environmental conditions, such as temperature, precipitation, and the frequency of natural disasters (Heidenreich and Seidel 2022). These factors significantly shape forest structure and influence growth, regeneration, and carbon storage capacity (Montesano et al. 2014; Heidenreich and Seidel 2022). Basic Lidar metrics calculated from ALS, such as point cloud density (the number of points per unit area) and total point count, can be used to model forest structure and are influenced by factors such as scanning speed and laser frequency (Petras et al. 2023). Higher point densities are generally considered indicative of higher quality scans (Kodors, 2017).

Accurate forest management requires reliable data on key forest inventory metrics including DBH, tree height, stem count, and volume. These measurements are essential for estimating AGB, which in turn informs carbon sequestration models and helps predict forest responses to climate change (Donager, Sánchez Meador, and Blackburn 2021; Chojnacky 2012). Despite the importance of these data, boreal forests remain underrepresented in global biomass studies because of the lack of precise, large-scale measurements (Chi et al. 2015). Given that approximately half of a tree’s biomass is carbon, accurate forest biomass data are crucial for the development of effective climate models (Wagers et al. 2021).

Biomass estimates are essential for understanding carbon storage and the broader carbon cycle, especially in the context of climate change (Chojnacky 2012). Forest biomass serves as a key indicator of carbon sequestration, helping policymakers assess the role of forests in mitigating climate change and predicting shifts in carbon stocks due to deforestation, forest growth, and land-use changes. This is particularly important in Alaska's boreal forests, which store significant amounts of carbon in both vegetation and soils. Allometric models enable efficient biomass estimation without destructive sampling, making them ideal for large-scale forest inventories. Several assumptions underlie the application of this method. First, biomass estimates rely on species-specific regional allometric equations, assuming that these models are applicable across the specific Alaskan ecoregion. Figure 2 shows how Alaska is divided into ecoregions (Nowacki and Brock 1995). Because Alaskan boreal forests face rapid warming, altered fire regimes, and permafrost thaw, accurately estimating biomass is critical for quantifying potential carbon emissions and evaluating the impacts of climate change. Accurate biomass measurements are also critical for biodiversity conservation as they help in understanding ecosystem health and resilience. These insights support conservation efforts in wilderness areas, and can guide strategies to enhance forest resilience to climate change, ultimately protecting biodiversity and ecosystem services in vulnerable regions.

This study used the open-source software Spanner (Sánchez Meador, Donager, and Cannon 2022), which is both cost-effective and flexible, for processing ground-based and airborne Lidar data. The use of such software is necessary to develop a standardized and scalable protocol that can be implemented in national forest inventory efforts. By improving the efficiency and accessibility of Lidar data processing, this study aims to enhance forest biomass estimation methods and support long-term forest management and carbon sequestration strategies across large, diverse landscapes such as Alaska's boreal forests. By offering detailed insights into the

relationship between forest structure and climate change, this research will have a broader ecological impact by informing policymakers on sustainable forest management practices.

1.6 Goals and Objectives

This study addresses the application of terrestrial laser scanning in dense boreal forests to estimate individual tree AGB. While ALS is suitable for large-scale forest inventories, TLS provides the fine-scale detail necessary for precise biomass measurements. This project establishes a baseline for future TLS measurements in Forest Inventory Analysis (FIA) plots, facilitating the long-term monitoring of boreal forest structure and its response to climate change.

1.6.1 Goals

The primary goal of this study was to assess the effectiveness of Terrestrial Laser Scanning (TLS) technology in measuring forest structural metrics and estimating aboveground biomass (AGB) in boreal forests. By establishing a baseline for TLS measurements in Forest Inventory Analysis (FIA) plots, this study sought to improve the accuracy of biomass estimates, which are crucial for understanding forest dynamics in the context of climate change.

1.6.2 Objectives

This study has three key objectives:

- Develop a Methodology for Future Monitoring: Establish a standardized protocol for integrating TLS into forest inventory assessments, enabling future research on the impact of climate change on boreal ecosystems.
- Calibrate a Model to Predict Species: Use Forest structural metrics to train a random forest model to predict tree species.
- Improve Biomass Estimates: Derive AGB estimates for individual trees from segmented TLS scans.

1.7 Assumptions and Limitations

This study operates based on key assumptions and acknowledges several limitations that influence the scope of its findings. It is assumed that GPS and georeferencing methods used in both TLS and MLS scans are sufficiently accurate to match detected trees with those measured in FIA data, despite the challenges posed by lower positional accuracy in MLS devices. Additionally, biomass estimates depend on the assumption that the allometric equations are suitable for the specific region in Alaska. Additionally, this study presumes that using multiple TLS scan positions will reduce occlusion in dense forest plots, although some sections of the upper canopy may still be missed.

This study also recognizes limitations, particularly in automated tree segmentation, which makes it difficult to accurately distinguish individual trees in dense canopies, leading to variability in detecting trees and estimating structural metrics. Aligning tree positions in point clouds with those measured by FIA is limited by the accuracy of segmentation, which may cause misalignment. Errors in detecting and estimating structural metrics such as DBH and height vary by forest type, which may limit the broader applicability of the results across different forest environments. Biomass estimates based on allometric equations may not fully capture regional variations in forest characteristics, especially given the unique environmental conditions in interior Alaska.

2 Methodology

2.1 Study Areas

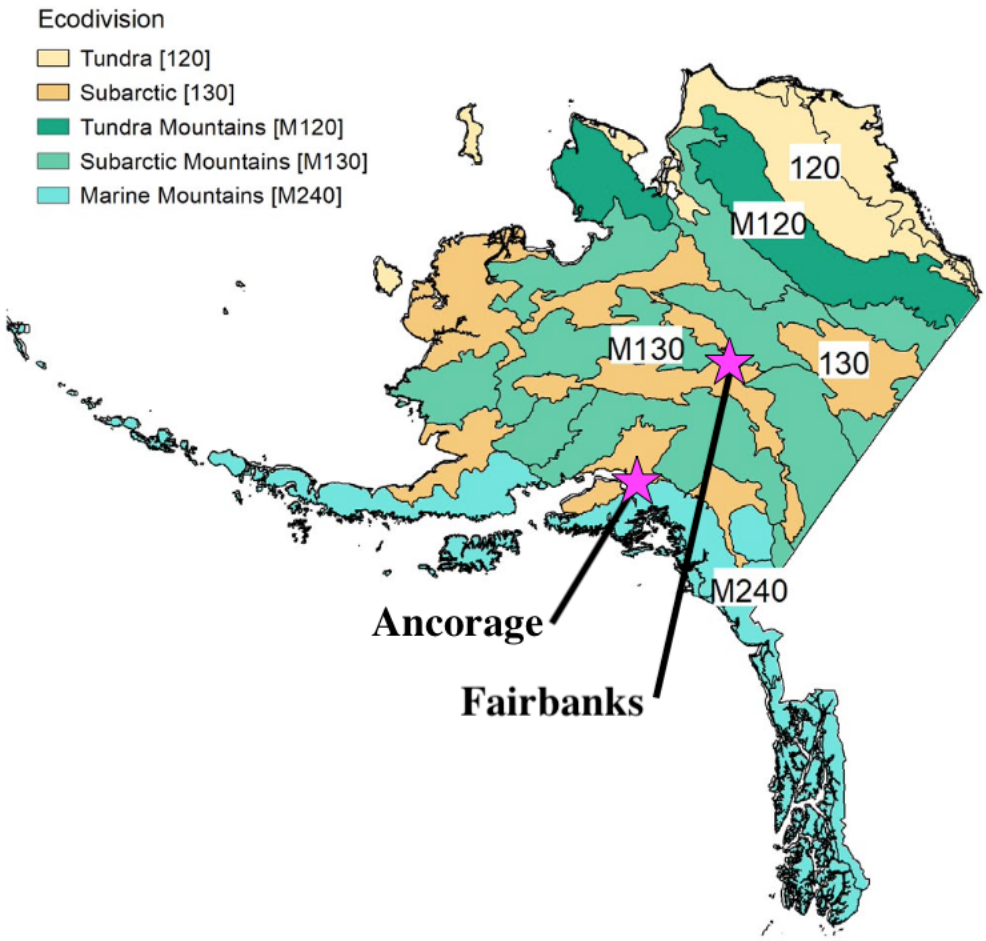

Figure 2: Map of Alaska ecodivisions (Nowacki and Brock 1995). Anchorage and Fairbanks are marked.

2.1.1 Anchorage

The first field season for this study was in the Campbell Tract Special Recreation Management Area (CTRA), adjacent to Far North Bicentennial Park in Anchorage Alaska (Figure 2). Fieldwork was conducted between September 12th and September 23rd, 2022. Campbell Tract, managed by the Bureau of Land Management, covers 730 acres of forest and was selected for its accessibility and tree species representative of typical boreal ecosystems found across interior Alaska ("Campbell Tract Special Recreation Management Area," n.d.). CTRA has FIA training plots that were established 10-12 years ago and resampled on the FIA time frame. All protocols used to sample the training plots were consistent with FIA on-grid plots; however, they were not subject to the strict confidentiality of the on-grip plots. The training plots were equivalent in quality and characteristics to the standard FIA plots. FIA field data used in this project were collected during the summer of 2022. Both FIA and Lidar field crews were in the field at the same time.

2.1.2 Fairbanks

The second sampling period was in the Bonanza Creek Experimental Forest (BCEF) outside Fairbank Alaska (Figure 2), for six weeks between June and August 2023. These sites were chosen for their accessibility from the city of Fairbanks, the presence of pre-established FIA plots, and the fact that the ecological gradient across the parks is archetypal of interior Alaska's boreal forests ("Study Sites & Design: Bonanza Creek Experimental Forest" 2002). At the BCEF, there are statistically sufficient field plots and airborne scans to represent interior Alaska's boreal forests, allowing us to apply small-sized sampling to a regional scale. Comparable FIA field data for this area was collected in the summer of 2023. Both FIA and Lidar field crews were in the field at the same time.

2.2 Data Collection

2.2.1 Field Data

In the FIA protocol, each plot is composed of four subplots arranged in a cluster, with subplot 1 at the center and the other three positioned 36.6 meters away at azimuths of 360°, 120°, and 240 ° magnetic north (Appendix A. Figure 14). Each subplot has a radius of 7.32 meters, covering an area of approximately 0.016 ha. Within each subplot is a microplot with a 2.07 meters radius. Each microplot is positioned 3.66 meters from the subplot center at a 90-degree azimuth from the subplot reference direction (Schulz 2014; "FIELD INSTRUCTIONS FOR THE ANNUAL INVENTORY OF ALASKA" 2020; Blehm, Ave, and Paul 2010).

The field methodology involves collecting detailed measurements of trees and forest conditions. The diameter at Breast Height (DBH) of trees is measured 1.35 meters above the ground, providing a standardized diameter measurement for each tree. If obstructions, such as branches, are present at this height, adjustments are made, and measurements are rounded to the nearest 0.1 inch (FIA protocol uses imperial, measurements have been converted to metric for this study). FIA uses imperial units that were converted into metric for this study. Only trees with a DBH of 12.7 centimeters or more are measured across the plot by FIA. Within the microplot, trees between 2.54 and 12.69 centimeters are measured. On the corresponding FIA plot, 206 trees were manually measured, 59 of them met the micro plot requirements. Tree height is recorded from the base to the top of the tree, and slope corrections are applied in areas with uneven terrain to ensure accuracy (Schulz 2014; "FIELD INSTRUCTIONS FOR THE ANNUAL INVENTORY OF ALASKA" 2020; Blehm, Ave, and Paul 2010).

Tree mortality is documented by identifying dead trees with a diameter of at least 12.7 centimeters that have been standing within the past five years, 29 dead trees were identified. The cause of death, such as insects, disease, or fire, is also noted. Tree density is calculated by measuring the number of trees per unit area, which helps assess forest structure and the effects of natural disturbances, such as wildfires or insect outbreaks ("FIELD INSTRUCTIONS FOR THE ANNUAL INVENTORY OF ALASKA" 2020; Blehm, Ave, and Paul 2010).

Tree location is mapped using azimuth and horizontal distance from a central point in the plot, enabling accurate monitoring of tree positions over time. Additionally, FIA crews recorded the species composition, identified the dominant species in each plot, and classified the forest type. The stand size class, from seedlings to mature trees, is noted to categorize the developmental stage of the forest. Finally, tree biomass is calculated to estimate the amount of carbon stored, providing insights into the forest's role in carbon sequestration and climate

change mitigation (Chojnacky 2012; “FIELD INSTRUCTIONS FOR THE ANNUAL INVENTORY OF ALASKA” 2020; Schulz 2014).

In Alaska, regional classification of vegetation is based on a hierarchical system tied to the U.S. National Vegetation Classification. Some of the primary forest macro-groups in Alaska include the Alaskan-Yukon North American Boreal Forest, dominated by black spruce, white spruce, and birch; the Alaskan-Yukon Boreal Mesic-Moist Black Spruce Forest, characterized by moist soils and dense black spruce stands; and the North American Boreal Subalpine & Subarctic Woodland, which includes a mix of black spruce and subarctic woodland species (Schulz, 2014). In this study, we focused on the Alaskan-Yukon North American Boreal Forest, which is dominant across our study sites. This classification can be divided into three categories: black spruce, deciduous, and mixed. Deciduous Forests have paper birch and black cottonwood as the dominant species and a more open understory (Figure 3.1. ab). Black Spruce forests are dominated by black spruce trees, which are characteristically dense with small trees and intersecting branches (Figure 3.2. ab). Mixed forests have an assortment of deciduous species, such as paper birch and cottonwood, with conifers, such as white and black spruce (Figure 3.3. ab). Forest Type was determined for each plot based on the dominant species composition of FIA measured trees. Species are not homogenous across plot, forest type is a general structure rather than an exact measurement (Schulz 2014; “FIELD INSTRUCTIONS FOR THE ANNUAL INVENTORY OF ALASKA” 2020).

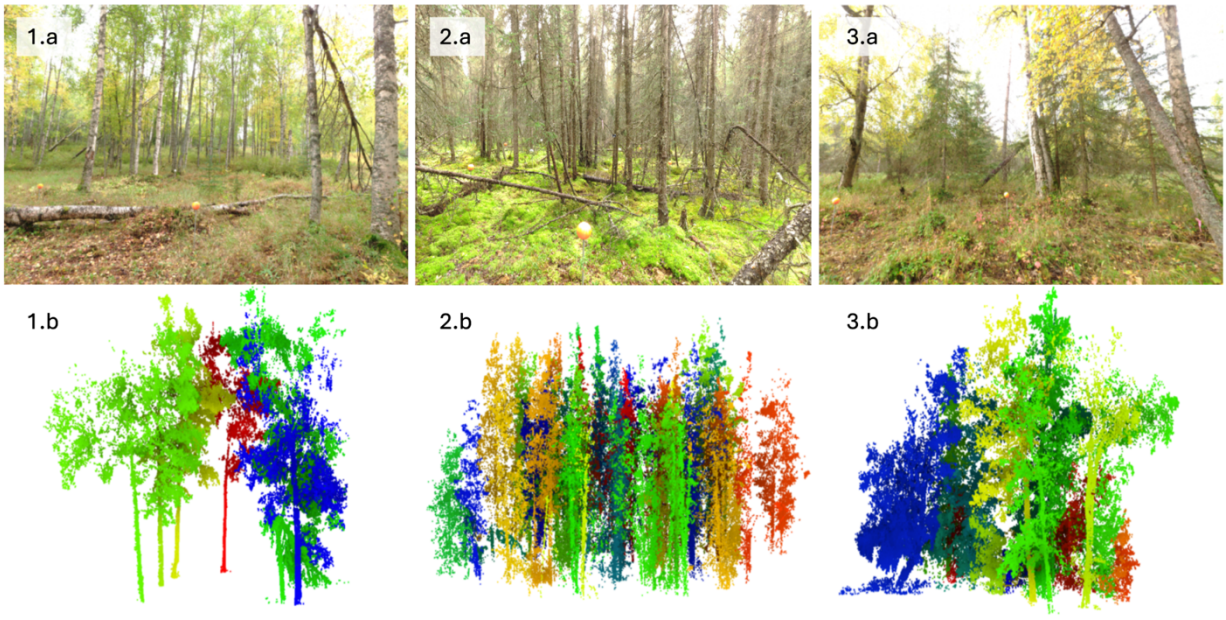

Figure 3: Forest Type: 1. Deciduous, 2. Black Spruce, 3. Mixed Forest. a are photographs taken by the Faro, b are segmented Lidar point clouds displayed in Cloud Compare. Orange and white target orbs can be seen in photographs.

2.2.2 Lidar

The study employed multiple modes of Lidar scanning technologies, including Terrestrial Laser Scanning (TLS), Mobile Laser Scanning (MLS), and Airborne Laser Scanning (ALS) to collect data on forest structure. During the 2022 field season in Campbell Tract Special Recreation Area (CTRA), seven plots were sampled using two mobile scanning devices, the ZEB Horizon (“ZEB-HORIZON User Manual v1.3” 2020) and Leica BLK2GO (“Leica BLK2GO User Manual Version 0.9,”

n.d.), alongside one stationary terrestrial scanner, the Faro Focus S350 ("Focus Premium and Focus Core User Documentation" 2022). Each plot was scanned by every device, although not every subplot was covered by each device owing to time constraints. In the Bonanza Creek Experimental Forest (BCEF), 43 plots were scanned using the Zeb Horizon.

2.2.2.1 Terrestrial Laser Scanning

Two TLS scanners, the FARO Focus S360 and the Leica BLK 360 were employed to collect detailed forest structure data in the Campbell Tract Special Recreation Area (CTRA). The Faro Focus S360 Laser Scanner is a phase-shift stationary lidar device. It has a range of up to 350 m, with a data collection rate of up to two million points per second. It features a 360° horizontal and 300° vertical field of view, with an accuracy of ± one millimeters at ten m and or minus two mm at 20 meters. The horizontal and vertical scan line densities take one scan line for every 0.035° horizontal or vertical increment, respectively. While scanning, the Faro collects a 360-degree panoramic photograph of its surroundings, which can be used to colorize the point cloud. This high-precision 3D scanning capability allowed for rapid collection of dense point clouds across the subplots, ensuring detailed coverage of the forest structure. The scanner's wide field of view and portability were essential for efficiently capturing the complex vegetation in the study area.

The Leica BLK360 is a compact, high-speed, time-of-flight stationary lidar device. It has a maximum range of 60 meters, with a scanning rate of up to 360,000 points per second, ensuring efficient data collection for small to medium-sized areas. Its field of view includes a full 360° horizontal and 300° vertical coverage, enabling comprehensive environmental scans. The scanner achieves a range accuracy of ± four millimeters at ten meters and ± seven millimeters at 20 meters, with beam divergence of 0.4 mrad. The BLK360 includes integrated high dynamic range (HDR) cameras that capture 360° panoramic images, which can be used to colorize the point cloud for enhanced visualization. The system's scan line density allows for adjustable resolution, supporting fast, standard, or high-density settings ("Leica BLK360 User Manual Version 4.0," n.d.).

A total of 113 scans and scanner-acquired 360-degree images were collected using the Faro Focus S360, with four to seven scans performed per subplot, covering 20 subplots in total. The Leica BLK360 was used to collect 26 scan one for each subplot with a single scan taken at subplot center. Target orbs were set up as Ground Control Points (GCPs), to ensure accurate stitching of the scans during preprocessing. The target orbs were 3D-printed orbs, 145 mm in diameter, mounted on a two-meter conduit (Appendix A. Figure 15). If the plots had substantial shrub vegetation to completely obscure the orbs from view, then a five-meter conduit was used strategically to raise the target orbs above the obstructing vegetation. The orbs are colored either white or orange to ensure high visibility during the stitching process. Depending on the vegetation density and potential obstructions on the plot, five to eleven target orbs were installed per subplot, including target orbs at the farthest North and South points on the plot. Table 1 shows the number of orbs that were set up and the number of scans taken for each plot subplot. For the target orbs to be effective, each point had to be visible from at least two scan positions, and each scan required visibility of at least three target orbs. Figure 15 in Appendix A. shows a conceptual model of the orb and scanner positioning. In Figure 3: 1.a, 2.a, 3.a, orange and white orbs are visible in the photo, white orbs are used to mark the North and South ends of the plot.

Table 1: Plots Scanned in Anchorage with TLS.

Plot	Forest Type	Scans Collected With FARO	Orbs on Plot	Subplot	Density Threshold	Eigen Threshold	Tree Count FIA	Tree Count microplot FIA	FIA Tree Count Estimate	Tree Count TLS
28	Deciduous	6	6	1	0.6	0.5	4	0	4	5
	Mixed	7	6	2	0.5	0.7	9	2	34	9
	Deciduous	4	5	4	0.6	0.7	2	0	3	2
40	Black	6	11	1	0.2	0.7	19	12	169	47
	Spruce	7	11	3	0.2	0.7	24	7	111	36
		7	11	4	0.2	0.7	22	12	172	41
48	Black	6	7	1	0.2	0.7	20	6	95	26
	Spruce	6	7	2	0.2	0.7	11	7	98	30
88	Mixed	5	6	1	0.2	0.7	15	1	27	23
		5	6	2	0.5	0.5	8	0	8	10
100	Mixed	5	7	1	0.4	0.5	8	2	33	15
		5	7	2	0.6	0.4	5	0	5	6
		4	7	3	0.4	0.5	11	1	23	12
116	Mixed	4	5	1	0.4	0.5	4	2	29	10
		4	6	2	0.5	0.5	2	0	2	4
		6	9	3	0.6	0.4	9	0	9	13
148	Mixed	7	9	1	0.2	0.7	15	3	52	28
		5	9	3	0.3	0.8	4	0	4	6
		5	9	4	0.3	0.8	10	4	60	10

2.2.2.2 Mobile Laser Scanning

In CTRA, each subplot was scanned twice with each MLS instrument, using different path types to compare the sampling methods: the lawnmower path and the triangle path. Both paths followed the bounds of a square superimposed on the circular subplot. For the triangle path, the user began at the subplot center and walked in a triangular formation around the subplot (Appendix A: Figure 14 A). For the lawnmower path, the user started at the center and walked to the southeast corner outside the subplot, following a striped pattern (Appendix A: Figure 14 B). Both path types rely on loop closure to minimize drift errors. When the MLS scanner is returned to a previously scanned position, the SLAM algorithm is able to reconcile trajectory errors. In CTRA 36 subplots were scanned with Leica BLK2GO and 37 with ZEB Horizon (Appendix B: Table 5). For plots already sampled by TLS, we left the GCPs in place for MLS scans. Otherwise, the GCPs were installed at the subplot center and the farthest north point. In Bonanza Creek Experimental Forest (BCEF), 165 subplots were scanned using the ZEB Horizon.

The Leica BLK2GO and ZEB Horizon were selected for this study based on their portability and ability to capture high-resolution 3D point clouds in challenging field conditions. The Leica BLK2GO collected data at 700,000 points per second with positional accuracy of 1–3 cm, featuring a 360° horizontal and 300° vertical field of view, making it ideal for comprehensive coverage of large-scale environments (Leica Geosystems). The ZEB Horizon, with a slightly lower point density of 300,000 points per second but the same positional accuracy of 1–3 cm, offered advantages for confined and complex environments (GeoSLAM). This made it especially suitable for navigating forested areas with restricted access. The combination of these two devices allowed for detailed and flexible data collection across study sites.

2.2.2.3 Aerial Laser Scanning

ALS scans were collected using NASA Goddard's Lidar, Hyperspectral, and Thermal (G-LiHT) airborne imaging system (Cook et al. 2013), which has been flown extensively over Southern and Interior Alaska, including the Campbell Tract Special Recreation Management Area (CTRA) and Bonanza Creek Experimental Forest (BCEF) during the summer of 2022. The G-LiHT system, equipped with a Riegl VQ-480 Airborne Laser Scanner, flew at an altitude of 335 m above ground level (AGL), collecting data at a pulse repetition rate of up to 300 kHz, yielding 150,000 points per second. Point spacing was 0.23 meters along flight lines and 0.57 meters between lines, providing a detailed point cloud with a 10 cm laser footprint, ideal for detecting fine-scale vegetation structure. The vertical accuracy was maintained at 10 cm, with GPS and Inertial Navigation System (INS) ensuring precise georeferencing. ALS data for all seven plots and 27 subplots (one subplot fell outside the G-LiHT flight path) were clipped to match the subplot boundaries in R Studio for subsequent analysis. The high point density and detailed canopy structure data captured by G-LiHT provided robust data for mapping forest characteristics across the study sites.

2.3 Processing

2.3.1 Terrestrial Laser Scanning

TLS scans were processed using SCENE (“SCENE” 2019), Faro’s proprietary software for handling .fls files from Faro devices (Figure 4.B.1). The initial steps involved colorizing the point clouds and applying standard SCENE distance (at 25 meters) and stray-point filters (minimum 6 neighboring points within 0.1 meters) to clean the data. The scans were manually registered for each subplot by identifying the target orbs visible in the scans. The locations of the North and South target orbs were recorded for each plot. Once all scans within a subplot were successfully registered, they were merged into a single point cloud for each subplot and exported as las files for further analysis. In CloudCompare (“CloudCompare v2.13.Beta” 2024), an open-source software for point cloud manipulation, the point clouds were normalized for point density by taking a subsample at a one cm resolution. This is a common step for TLS multi-scans to remove redundant or overlapping points caused by the combination of several dense scans. The subsample also makes the file size more manageable for processing, without losing details.

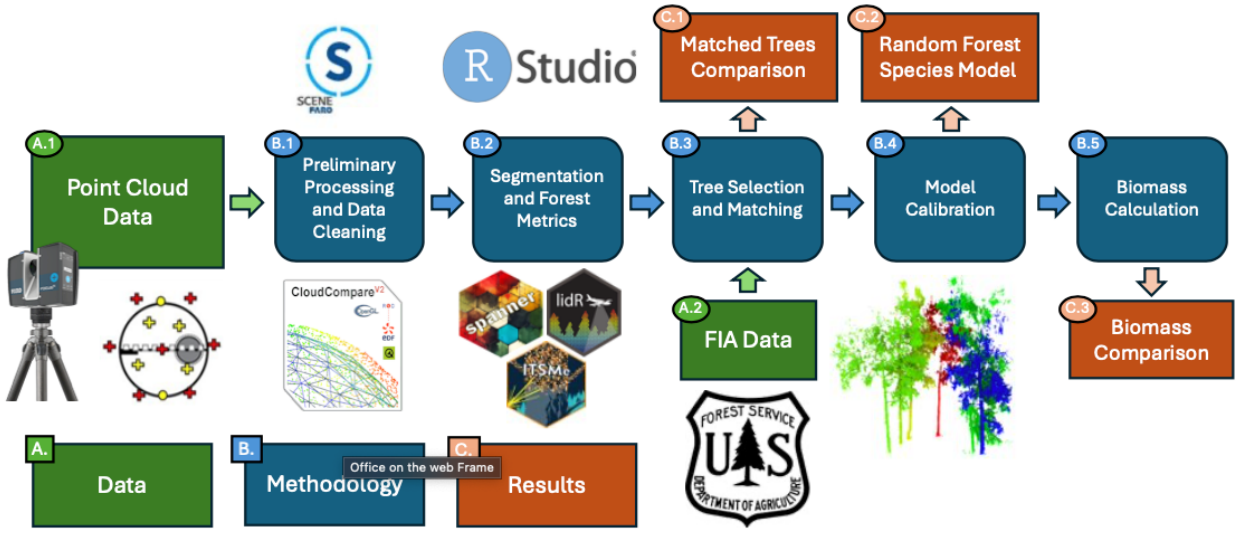

Figure 4: Conceptual Model. Divided into A. Data, B. Methodology, and C. Results. A. Data represents the data sources for this study, A.1 is Point Cloud Data collected by TLS and A.2 is FIA Data manually collected. B. Methodology is split up into five primary steps taken including B.1 Preliminary Processing and Data Cleaning, B.2 Segmentation and Forest Metrics, B.3 Tree Selection and Matching, B.4 Model Calibration, and B.5 Biomass Calculation. C. Results shows the three primary types of results produces with C.1 Matched Trees Comparison, C.2 Random Forest Species Model, and C.3 Biomass Comparison. Bellow A.1 is a photo of the TLS FARO Focus device used in this study and a reference plot setup with yellow orb placement and red scanner placement. Above B.1 is the Faro Scene software logo, and below the CloudCompare software logo. Above B.2 is the RStudio logo and bellow three logos for the R Packages: Spanner, lidR, and ITSMe. Bellow A.2 is the Forest Service logo. Bellow B.4 is an example of a segmented TLS point cloud.

2.3.2 Mobile Laser Scanning

BLK2GO scans were imported into Cyclone, Leica software for converting LGS files to E57 or las formats. Similarly, ZEB Horizon scans were processed using GeoSLAM Connect, GeoSLAM's proprietary software, which was required to convert .geoslam files to las files. Once converted, the MLS files were imported into Cloud Compare ("CloudCompare v2.13.Beta" 2024), and georeferenced to their respective ALS files for each subplot.

While developing the field sampling protocol and initial processing of MLS data was withing the scope of this thesis work, further analysis and deriving individual tree metrics is the purview of future work. This future work will include investigation into the merging of the terrestrial lidar with the aerial lidar for more landscape level analysis. The higher fidelity TLS data from the FARO scanner is the focus of the analytical work done here.

2.4 Segmentation and Forest Metrics

The rest of the processing and analysis is performed in R Studio, an open-source software for R, a programming language for statistical computing and graphics (R Core Team 2024). The R package Spanner (Sánchez Meador, Donager, and Cannon 2022; Donager, Sánchez Meador, and Blackburn 2021), was used to segment individual trees from Lidar-derived point clouds, facilitating forest structure analysis. Spanner identifies and segments trees using a combination of geometric and topological techniques. The segmentation process begins by normalizing the point cloud to remove the effects of terrain and topography, followed by the removal of ground points to focus solely on tree structures. Once the ground points are filtered out, eigenvalue-based rasterization is applied to assess the verticality and density of points within the cloud to

detect potential tree boles. After bole detection, the RANSAC algorithm fits cylinders to accurately model the tree trunks (Donager, Sánchez Meador, and Blackburn 2021).

Automated tree segmentation from Lidar data is not perfect, with challenges in distinguishing individual trees in dense or overlapping canopies, leading to variability in tree detection and structural metric estimates. To optimize the segmentation process, two key parameters were adjusted: the eigen threshold, which controls the verticality of the points, and the density threshold, which determines the minimum point density required for inclusion in the rasterized output. These adjustments were fine-tuned for each subplot through iterative testing and visualization in Cloud Compare ("CloudCompare v2.13.Beta" 2024), cross-referenced with 360-degree photos taken by the FARO scanner. Table 1 lists the density threshold and eigen threshold used for each plot subplot. Increasing the eigen threshold helped the algorithm detect vertical boles more effectively but setting it too high caused smaller trees to be missing. Similarly, setting the density threshold too low resulted in over-segmentation (excessive splitting of trees), whereas a high threshold caused under-segmentation (failing to detect trees accurately).

Once the individual tree point clouds were obtained from Spanner, the ITSME (Terryn et al. 2023) R package was used to calculate additional structural metrics. ITSME specializes in processing individual tree point clouds to derive forest metrics, such as tree height, projected crown area (PA), and 3D alpha crown volume (ACV). Tree height was calculated as the difference between the highest and lowest points in the tree's point cloud, whereas the projected area was computed as the area of the concave hull created around the crown. The 3D alpha volume, a measure of the crown volume, was also generated using ITSME's alpha shape algorithm (Terryn et al. 2023).

Both Spanner and ITSME were used to extract five essential forest metrics, including DBH and tree location from Spanner and height, alpha volume, and projected area from ITSME, providing a broad assessment of tree structure.

2.5 Tree Matching

Trees measured by the Forest Inventory and Analysis (FIA) program were matched with those detected by the Faro scanner. Because FIA only measures trees with a diameter at breast height (DBH) greater than 12.7 cm across the whole subplot, the Faro scanner, which captures all objects within the scan area, detected more trees than FIA. The first step in the matching process was to compile all location data and select only the trees located within 8 m of the subplot center. Although the radius of the subplot was 7.3 m, an 8-meter limit was used to include trees on the edge, allowing for a margin of error in the matching process. This dataset formed the basis for further analysis.

Once all on-plot trees were selected, the tree locations were converted to a local coordinate system, where the subplot center was positioned at (0,0). The conversion was performed using the North and South target orb locations. FIA tree locations, which were documented using azimuth and distance from the subplot center, were also transformed into the same local coordinate system, enabling direct comparison. Three of the FIA trees did not have distance from center data recorded and had to be removed. Additionally, 59 FIA-recorded dead trees were removed from the dataset to eliminate a potential source of error in the matching process. Downed trees or partially standing dead, may potentially interfere with the matching process or calibrating the species prediction model. While the dead trees are removed from the

matching process and analysis, they are later incorporated for the FIA data biomass calculation. After cleaning the FIA dataset, there are 173 remaining trees for the matching process.

To further refine the TLS dataset and remove potential outliers, a plot of FIA trees by DBH and height was generated to establish the upper and lower bounds for these metrics (Figure 5). A 15% margin of error was applied to these bounds, and this threshold was used to filter the Faro dataset by removing small shrubs, stumps, and downed logs that would otherwise introduce additional errors into the matching process. Of the original 449 trees, 405 were within the adjusted bounds. The 44 trees outside the adjusted bounds were visually assessed and determined to be downed logs, stumps, shrubs, saplings, or stray branches that caused segmentation errors. Removing these was necessary to aid the next step when matching trees based on proximity. With the dataset cleaned, the FIA and TLS trees were matched by proximity, ensuring an accurate alignment between the two datasets for subsequent analysis (Figure 5).

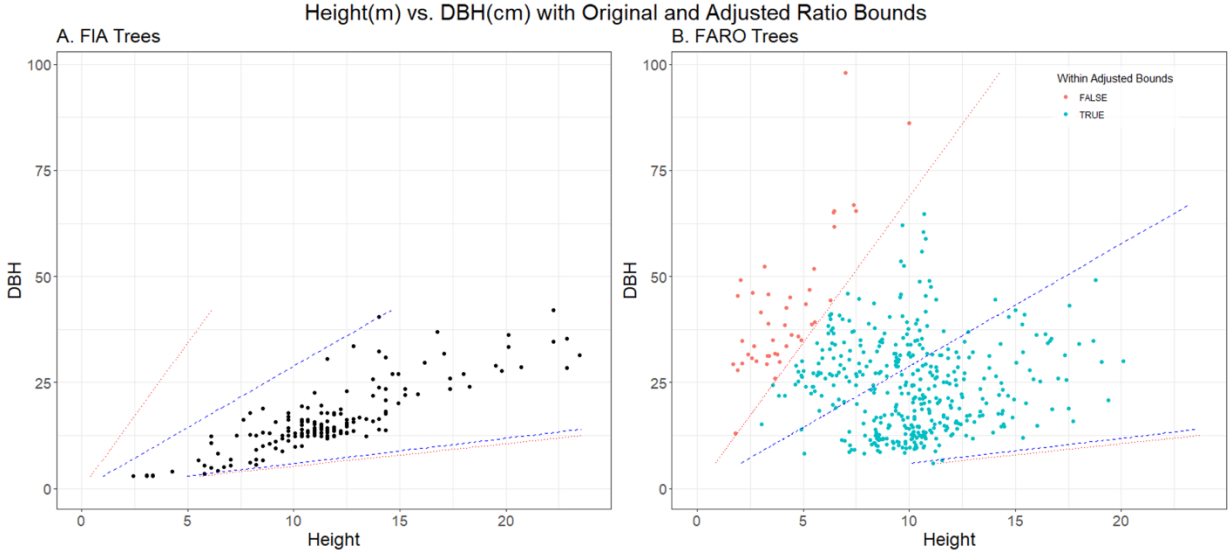

Figure 5: Scatterplots showing the ratio between Height and DBH for A. FIA trees and B. Faro trees. Blue lines represent the exact bounds of Height to DBH for FIA trees, red line is adjusted for a margin of error. In plot B. blue points are within the adjusted bounds and the orange ones outside.

Once the matching process was completed, the matches were evaluated based on proximity and height similarity, as well as visually assessed, as shown in Figure 6. Matches were labeled as either true or false. A true match was defined as a pair of trees whose locations were within two meters from each other, had less than 20 centimeters difference in DBH, and whose height difference did not exceed five meters. These were considered reliable matches, indicating a high degree of confidence that they represent the same tree. Conversely, false matches were those that did not meet these criteria, with significant differences in either location, DBH, or height, leading to lower confidence in the match being the same tree, there were 109 true matches and 64 false matches. A dataset of matched trees with comparable structural metrics was compiled and used to build the species prediction model. In addition, a dataset of unmatched trees detected by the TLS scanner was generated, consisting of trees that did not match any of the 173 FIA-measured trees.

Figure 6:Matching FIA and Faro trees by Plot Subplot, after converting all trees locations to a local coordinate system. Plots A, B, C are in deciduous forests, plots D, E, F, G, H, I, J are black spruce forests, and plots K, L, M, N, O, P, Q, R, S, are mixed forests.

2.6 Model Calibration

With a dataset of true matched trees between the FIA and TLS, which included species identification and structural metrics derived from the point cloud, a random forest (RF) model was developed to predict the species of trees in the unmatched TLS dataset. The initial set of structural metrics obtained from the TLS point clouds included DBH, height, projected area (PA), and alpha crown volume (ACV). In addition, ratio-based metrics were created by taking ratios between these primary metrics, resulting in 9 unique structural variables.

To optimize the RF model, Recursive Feature Elimination (RFE) was conducted to identify the most important variables for species prediction. RFE was performed using 10-fold cross-validation to assess the performance of the model across different subsets of variables. The results indicate that the best-performing model used five variables: PA, ACV/Height, height, ACV, and PA/height. These five variables were selected for training the RF model, as they showed the highest importance.

The dataset was then split into training (80%) and testing (20%) sets to validate the predictive accuracy of the model. A 10-fold cross validation with Synthetic Minority Oversampling Technic (SMOTE) was used on the training dataset. SMOTE is a data augmentation technique used to address class imbalance, in this study it was used to address the small sample size of paper birch to improve the classification performance. The RF model was trained using the five key variables identified by the RFE and tested different numbers of predictors sampled at each split set at two, six, and ten. The performance of the model was evaluated on both training and testing sets.

Once the RF model was validated, it was applied to both the unmatched and original TLS datasets. This allowed for the prediction of species for all segmented point clouds, including those without FIA matches, thereby providing comprehensive species identification for the entire set of scanned trees.

2.7 Allometric Equation for Biomass

To estimate above-ground biomass (AGB) for individual trees, the allometric equation employed in this research was:

$$AGBPredicted = a \times Db \times Hc$$

This equation predicts biomass based on tree diameter at breast height (DBH) and height (H), where a, b, and c are species-specific coefficients (Chojnacky 2012). These coefficients were derived from the Forest Inventory and Analysis (FIA) database and relevant literature, allowing for a standardized biomass estimation that takes into account the variability between different species. This allometric equation was used to calculate the AGB for several datasets. First, the biomass was calculated for individual trees with matching measurements in both the FIA and TLS datasets, allowing for direct comparison between the two methods. Additionally, biomass estimates were generated for all FIA-measured trees, including dead trees and snags, which play crucial roles in carbon cycling. The equation was also applied to all trees detected by TLS, including smaller trees that were not recorded by FIA due to size limitations. Furthermore, biomass estimates were calculated for unmatched trees in the TLS dataset that did not have corresponding FIA measurements. These estimates were derived under the assumption that the TLS system provided the necessary resolution and precision to capture forest structure, particularly for smaller trees not recorded by FIA (Chojnacky 2012).

The resulting biomass estimates from each dataset were then compared to assess differences in tree detection between FIA and TLS and to evaluate the overall contribution of smaller trees to the total biomass in the study area.

3 Results and Discussion

3.1 Tree Detection

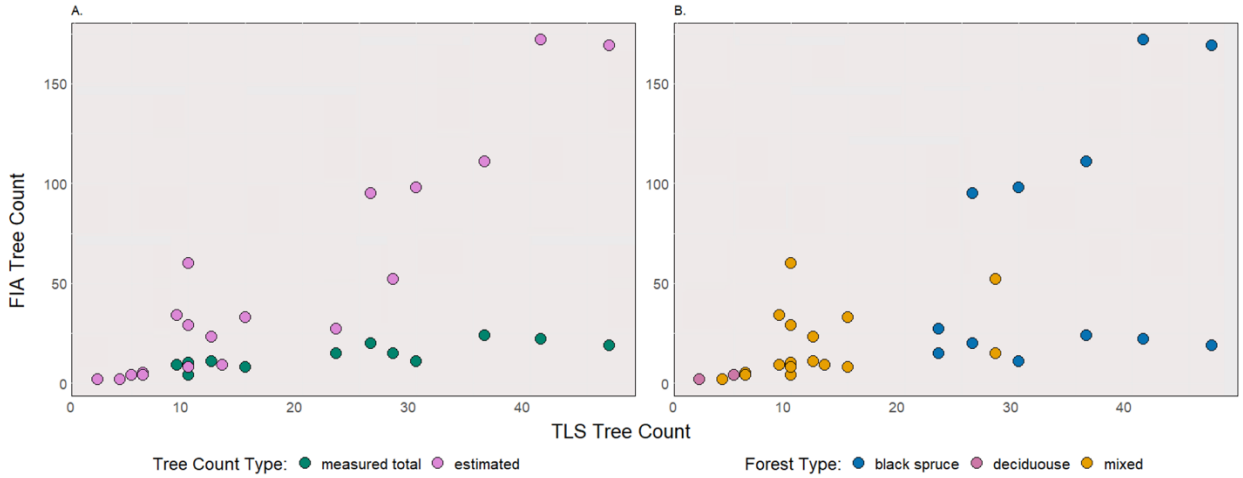

Figure 7: Tree Count between FIA measured trees and FIA predicted tree density with TLS detected trees for each plot. A. shows the difference between FIA measured trees and FIA predicted tree. B. shows the forest type.

The TLS consistently detected more trees than were directly measured by FIA across all plots and forest types, as shown in Figure 7. However, TLS detected fewer trees than FIA estimated would be present in the subplot based on their microplot small-tree estimation protocol. Figure 7A illustrates this comparison, showing the total tree counts measured by FIA, estimated by FIA, and detected by TLS. Figure 7B further breaks down the comparison of tree counts between FIA and TLS by forest type. Notably, black spruce forests consistently exhibited the highest total tree counts across all subplot, while deciduous forests had the lowest. These results align with the expectation that TLS would detect more trees than FIA's direct measurements FIA protocol only measuring trees with a DBH above 12.7 cm outside of the microplot. However, the discrepancy between TLS-detected trees and FIA-estimated counts suggests potential limitations in TLS detection or an overestimation in the microplot small tree estimates, particularly in dense forest environments. Density at any scale is not consistent across a wild forest making accurate tree count estimation involving scaling a small area difficult. This pattern is particularly evident in black spruce forests, which are characterized by high densities of small-diameter trees, however the microplot estimates predict most black spruce plots as having more than 100 to 170 trees in a 168 m^2 circle. Deciduous forests, with their typically larger and fewer stems, showed the smallest discrepancies between both FIA measurements and TLS. Both of the deciduous subplot and several of the more open mixed forest subplots have no trees on their microplot, as a result the microplot estimations show no small trees or saplings on the subplot.

3.2 Overview of Key Findings

This study identified significant discrepancies in biomass estimates between terrestrial laser scanning (TLS) and Forest Inventory and Analysis (FIA) manual measurements, mainly because TLS detects smaller trees that FIA does manually measure. Persson et al. (2022) also noted that TLS, particularly when combined with ALS, provides more accurate and time-efficient forest inventory results compared to traditional methods. TLS's higher biomass estimates were more pronounced in mixed and black spruce forests, with species and forest type influencing DBH, height, and biomass estimates (Åkerblom and Kaitaniemi 2021; Wardius and Hein 2024).

The comparison between matched trees (Figure 8) revealed significant differences in height and biomass between TLS and FIA measurements, depending on the species and forest type. DBH differences were significantly lower in deciduous forests than in black spruce and mixed forests, whereas height errors were notably higher for paper birch than for other species. Biomass differences were also visually greater in black spruce and mixed forests than in deciduous forests, indicating that deciduous forests had the lowest variability in biomass estimates (Figure 8 B.1 and B.3). These results highlight the influence of forest type and species composition on TLS-derived forest metrics.

The results of the correlation analysis showed a stronger correlation between DBH and biomass errors than height errors, indicating that DBH discrepancies have a greater impact on biomass estimation. Additionally, the lack of correlation between DBH and height errors suggests that the magnitude of these errors is independent of the tree size.

3.3 Matched Trees Comparison

The matching process between TLS detected and FIA measured trees consisted of converting all tree locations to a local coordinate system, aligning them based on proximity, height, and DBH, and determining the validity of the match. Matches with a Distance between tree locations greater than 2 meters, a height difference greater than 5 meters, or a DBH difference greater than 20 cm were determined as false matches as there was not enough confidence in the match to conclude they were the same tree. False matches needed to be excluded to effectively train the random forest model for species prediction and for the integrity of comparing individual trees. Of the 173 matches, 109 were classified as true (63%) and 64 false (36%). Out of the 173 FIA trees, 53 of them had a DBH less than 12.7 cm and were measured on the micro plot, while the remaining 120 were larger. The larger trees performed well in matching with 90 true matches (75%) and only 30 false (25%). The microplot trees did not fare as well with only 19 true matches (35%) and 34 false (64%). Further examining the 14 trees with a DBH bellow 6.3 cm, only 1 true match (7%) was found and 13 false (92%).

Using the FIA measurements as validation, the difference values between FIA and TLS for DBH, height, and biomass were calculated for each matched tree. The difference value showed the amount of error on an individual tree level between the FIA manually measured validation data and the TLS point cloud calculated metrics.

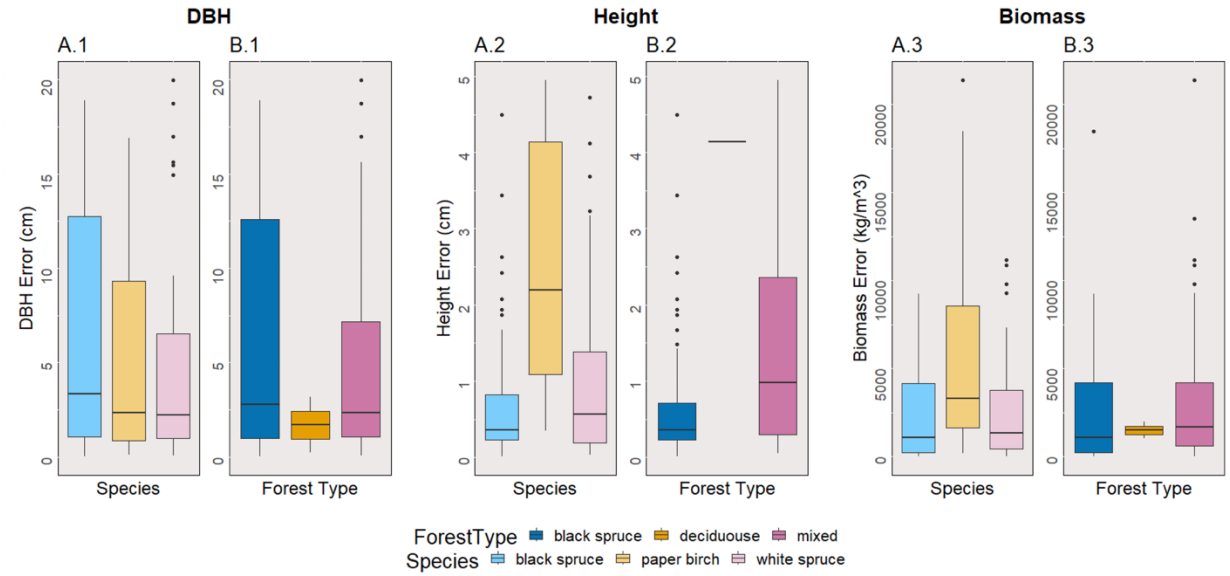

Figure 8: Figure 8: Structural metrics, DBH (.1) Height (.2), and Biomass (.3), between matched trees by Species (A) and Forest Type (B).

To evaluate these errors, normality tests were conducted to determine appropriate statistical methods for further analysis. Since the normality tests indicated that none of the metrics were normally distributed ($p < 0.001$ for all) and the sample size was relatively small ($n = 109$), the Kruskal-Wallis test was chosen because it is suitable for non-parametric data with unequal sample sizes (Kruskal and Wallis 1952). Additionally, assumptions for the Kruskal-Wallis test, including independence of observations and similar distribution shapes among groups, were verified. In cases of significance, the Kruskal-Wallis test was followed by Dunn's post-hoc test (Dunn, O. J. 1964). Correlation analysis was also conducted using the Kendall rank correlation test (Kendall, n.d.)to understand the relationship between DBH, height, and biomass errors. It was shown that DBH and height error had no correlation ($p = 0.251$), while DBH and biomass error had a strong positive correlation ($p < 0.001$) and height and biomass error had a weak positive correlation ($p = 0.019$). Biomass is calculated using a DBH and height in an allometric equation and a positive correlation is expected, however the different strengths indicates that DBH error may effect biomass error more than height error would.

3.3.1 DBH, Height, Biomass

The Kruskal-Wallis test revealed significant differences in height and biomass between the groups. Figure 8 shows the comparison of DBH, height, and biomass differences by species and forest type using box plots, providing a visual representation of these significant discrepancies.

Height error was analyzed using the Kruskal-Wallis test, which indicated significant differences by species ($p = 0.001$) with a moderate effect size ($\eta^2 = 0.135$) and by plot ($p = 0.004$). Dunn's test was then performed for pairwise comparisons between species, revealing that height differences were significantly greater for paper birch than for white spruce ($p = 0.004$) or black spruce ($p < 0.0002$), indicating that paper birch had notably higher height errors. However, there were no significant differences between the white and black spruce. A Kruskal-Wallis test for height error by forest type indicated a significant differences ($p = 0.012$), and a subsequent

Dunn's test also confirmed a significant difference in height error between black spruce and mixed forests.

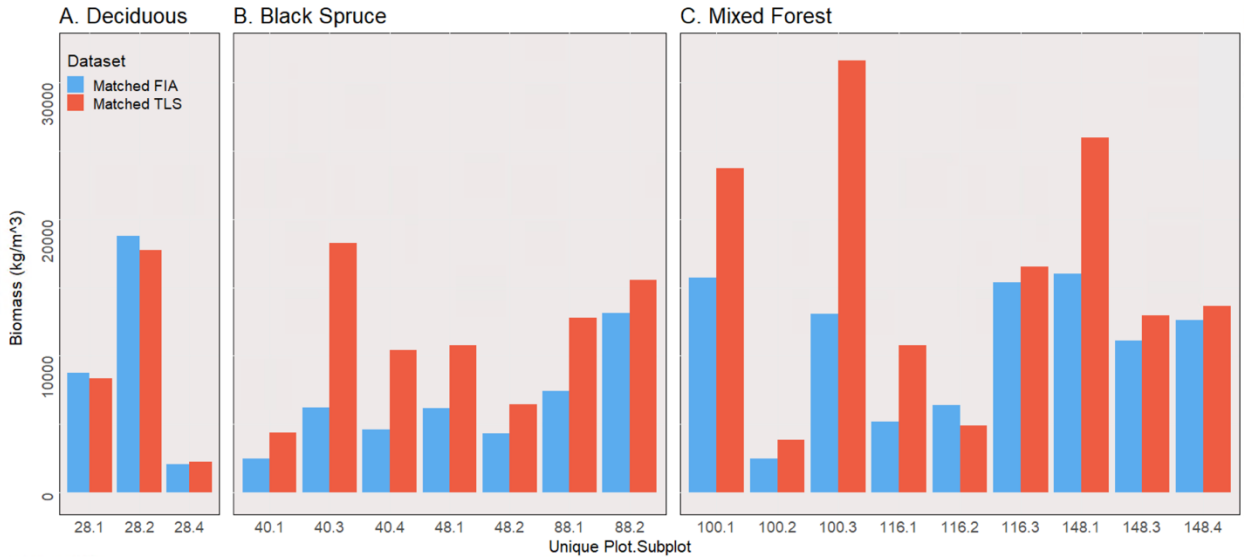

Figure 9: Total biomass by Plot Subplot (ex. 100.1 is plot 100 subplot 1), between matched trees by forest type.

Biomass error was also analyzed using the Kruskal-Wallis test, which revealed significant differences by species ($p = 0.048$), with a small effect size for biomass differences by species ($\eta^2 = 0.047$). Dunn's test for pairwise comparisons indicated that biomass differences were significantly greater for paper birch than for black spruce species ($p = 0.030$). However, no comparisons with other species were statistically significant. Biomass differences were not significant by forest type. This can be seen in Figure 9, where the biomass between matched trees is compared on a plot subplot basis.

These findings indicate that forest type and species composition significantly influence the error in forest structure metrics, such height, but have little effect on that of DBH and biomass, between TLS scans and FIA manual measurements. Biomass errors were particularly influenced by species, with black spruce showing more biomass variability than paper birch. Additionally, paper birch exhibited significantly greater height and biomass errors than other species. These results emphasize the need to account for species and forest type when calibrating and developing models to estimate forest structure metrics using TLS data.

3.3.2 Species vs Forest Type

In many studies, species have been shown to have a substantial impact on measurement errors in TLS scans (Terryn et al. 2020). Crown size, overlapping branches, and tree structure all play a role in the level of occlusion present in a TLS scan. Puletti et al. (2020) noted that Lidar's effectiveness can vary between broadleaf and needleleaf species, with greater occlusion issues observed for broadleaf species like paper birch, which aligns with the findings in this study. When comparing the amount of error between TLS- and FIA-measured trees, we found that out of the three species in this study, paper birch was the highest (Figure 8A). The Kruskal-Wallis test results showed that paper birch trees had significantly more errors in height measurements and exhibited larger biomass discrepancies than mixed and black spruce trees. Wagers et al. (2021) found that TLS provided better estimates of biomass for smaller black spruce trees compared to

traditional allometric equations, highlighting TLS's effectiveness in complex forest structures. The round, broad-leafed crown of deciduous trees, such as paper birch, may cause more occlusion compared to cone-shaped crowns of conifers, leading to increased height measurement errors (Puletti et al. 2020).

Puletti et al. (2021) highlighted that unique forest types such as beech and pine present distinct challenges for TLS-based measurements. In this study, the black spruce forests presented the greatest challenges to measure. The Kruskal-Wallis test results showed that DBH differences varied significantly, with black spruce and mixed forests showing greater discrepancies compared to deciduous forests (Figure 8B). Since biomass is calculated using a species-specific allometric equation based on DBH and height, it is expected that the relationships observed between DBH and height errors will also be reflected in biomass errors (Chojnacky 2012). Mixed forests exhibited the highest variability in biomass estimates, however both black spruce and mixed showed significantly more error in biomass than deciduous. Wagers et al. (2021) found that occlusion significantly affected TLS accuracy, particularly in dense black spruce stands.

In this study, there were a limited number of species and forest types, and two of the forest types, deciduous and black spruce, were characterized by being nearly homogenous in species composition. However, the differences in structural metrics measured in these near-homogenous forests and the species that compose them can indicate where some of the error originates. Black spruce forests showed little difference from the black spruce species measurements between matched trees (Figure 8). In contrast, there was a discrepancy in error measurement between the paper birch species and deciduous forest type when comparing DBH, height, and biomass error, as shown in Figure 8. This may be due to the measurements of paper birch in mixed plots, while black spruce species are less common in mixed plots due to their habitat preferences for cold wet forests (Wirth et al. 2008). The deciduous forests performed very well in calculating accurate DBH and biomass estimated from point clouds and were markedly better than paper birch species in height measurements. Conversely, a mixed forest with more species and structural variability had more error. TLS performs better in homogenous forest than in mixed forests when calculating structural metrics (Yrttimaa et al. 2020).

3.4 Random Forest Model

3.4.1 Model Performance

The Random Forest model for determining tree species using structural attributes showed an average accuracy of 7791% (Kappa: 0.65), on the cross-validation training dataset. The cross-validation training dataset is 80% of the matched trees. The number of predictors sampled at each split with the best-performance accuracy was ten. The training data producer’s accuracy for paper birch was 63.3% with 8 true positives, for black spruce it was 87.5% with 41 true positives, and for white spruce 63.3% with 29 true positives. Paper birch had the lowest producer’s accuracy and smallest sample size, SMOTE was applied to oversample the paper birch class improving the producer’s accuracy.

The testing dataset, the remaining 20% of the matched trees had an accuracy of 86.95% (Kappa: 0.78) showing substantial agreement. The improvement from training to testing accuracy suggests the model generalizes well to unseen data. The testing data producer’s accuracy for paper birch was 100% with 3 true positives, for black spruce it was 100% with 11 true positives,

and for white spruce 87.5% with 7 true positives. Black and white spruce had much higher producer's accuracy than paper birch.

3.4.2 Species Classification

Figure 10 depicts the species distribution across Plot Subplot from different datasets, TLS Detected (10A), FIA (10B), and Unmatched TLS Detected (10C). The performance of the random forest model can be visually evaluated in Figure 10 by comparing the distribution of species between different datasets for the same Plot Subplot. It is expected that these datasets will not line up perfectly; however, it can be inferred that the predicted tree species will have a similar alignment with the observed tree species in the same plots. In Figure 10C. shows that most of the unmatched trees were predicted to be black spruce, and the distribution of these black spruce trees provides confidence in the model's performance, as they are clustered in black spruce dominant plots. In addition, black spruce trees tend to grow slowly and cluster in dense forests with smaller stems because of their preferred habitat in poorly drained lowlands and north-facing slopes characterized by permafrost (Wirth et al. 2008). The growth tendencies of the black spruce mean they are often overlooked in FIA surveys that only measure larger trees.

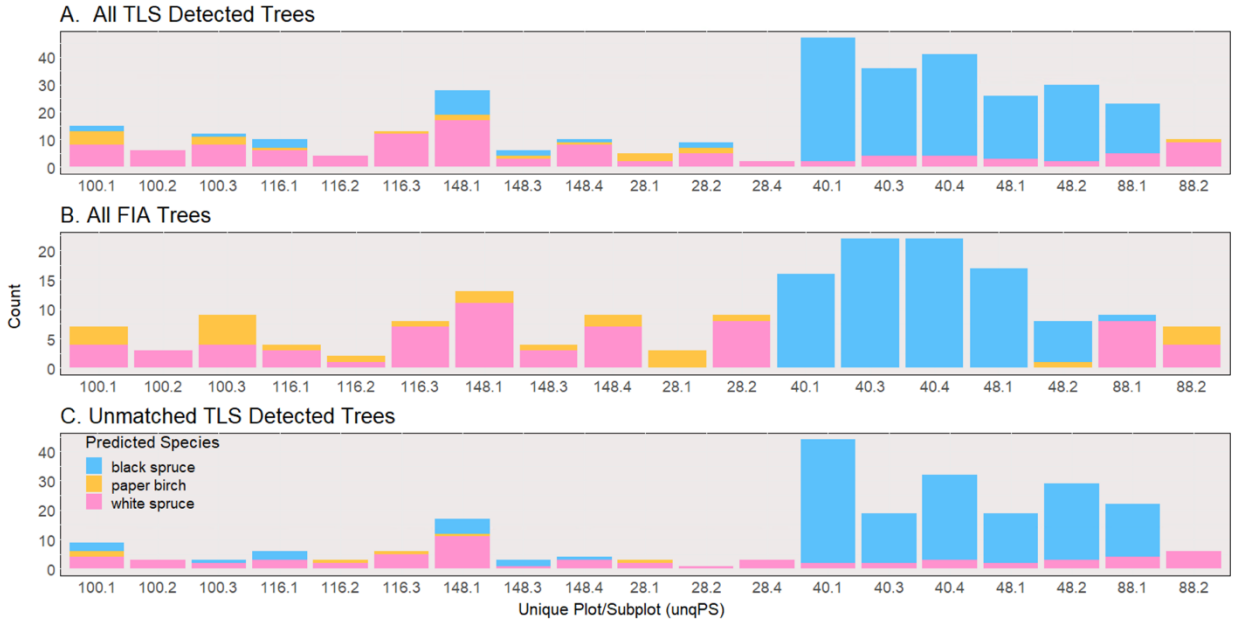

Figure 10:Species Distribution of black spruce, paper birch, and white spruce, across Plot Subplot (ex. 100.1 is plot 100 subplot 1) for Datasets: A. All TLS Detected Trees, B. All FIA Trees, and C. Unmatched TLS Detected Trees.

With regard to species identification using structural metrics, the point density of ALS data is often insufficient to capture the detailed geometric features required for accurate species classification (Persson et al., 2022). Terrestrial laser scanning (TLS) is a promising technique for species identification through structural metrics.

3.5 Biomass comparison

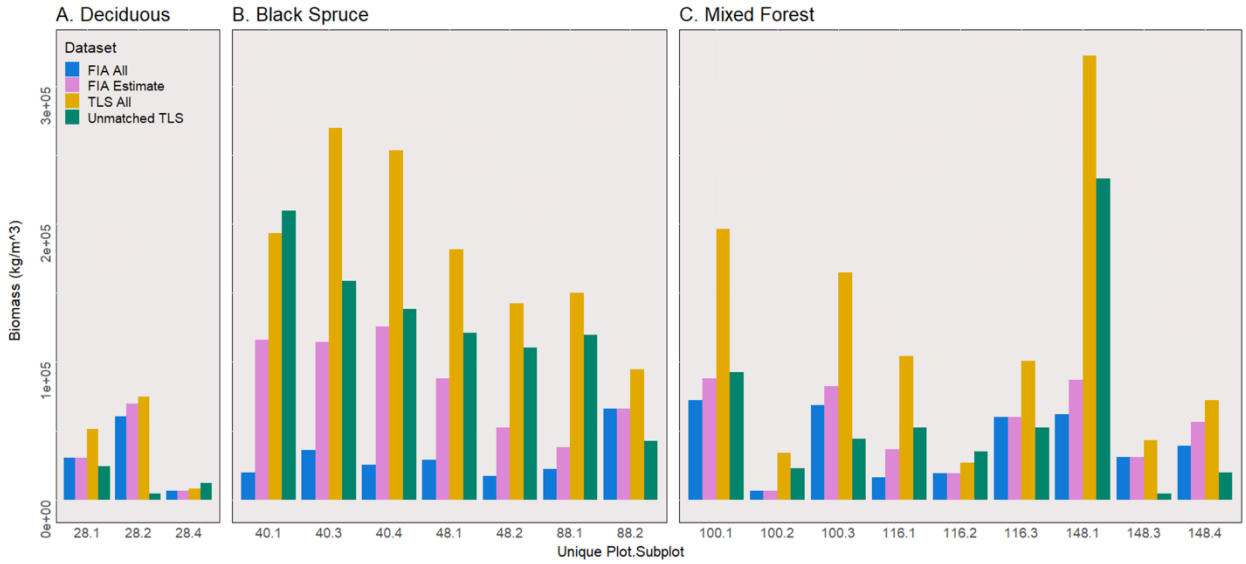

Figure 11: Total biomass estimates were compared across three categories: TLS All, FIA All, and Unmatched TLS, within the distinct deciduous, black spruce, and mixed forest type black spruce (A), mixed forest (B), and deciduous (C) for each Plot Subplot (ex. 100.1 is plot 100 subplot 1).

Figure 11 provides a visual comparison of aboveground biomass estimates from TLS All, FIA All, FIA Estimate, and Unmatched TLS split by plot and subplot for each forest type. FIA plots have a 7.32 meters radius, and the bar graph shows the amount of aboveground biomass calculated for each plot categorized by forest type. FIA All represents all trees measure by FIA including the dead trees and the microplot trees. FIA Estimate uses the microplot small tree estimates to estimate how much additional biomass there would be if all small trees on plot were measured by FIA. TLS All has all trees measured with FARO and within the adjusted bounds. Unmatched trees includes TLS trees from TLS All that were not matched with FIA trees.

A Wilcoxon signed-rank test (Wilcoxon, F. 1945), was conducted to compare the biomass values of TLS All and FIA All, TLS All and FIA Estimate, and Unmatched TLS and Microplot Estimate FIA, across the forest types. The results all revealed a statistically significant difference between the sets, with a V statistic of 190 and a p-value of 3.815e-06, indicating a notable shift in biomass between the two measurements.

Subsequently, a Kruskal-Wallis test was performed to assess differences in the biomass between TLS-measured trees and FIA-measured trees by Plot Subplot across forest type. The analysis yielded a chi-squared value of 9.863 with two degrees of freedom and a p-value of 0.007, suggesting that at least one forest type significantly differed from the others. Dunn's post-hoc test was conducted to further explore these differences. The results showed a significant difference between black spruce and deciduous forests (adjusted p-value = 0.019), and a significant difference between black spruce and mixed forests (adjusted p-value = 0.017). These differences can be observed in Figure 11, which compares the TLS and FIA datasets. Additionally, a pairwise comparisons using the Wilcoxon rank sum test was conducted, indicating no significant differences after FDR adjustment between black spruce and deciduous (p-value = 0.107) and between deciduous and mixed forests (p-value = 0.154), while there was a significant difference between black spruce and mixed (p-value = 0.015). Collectively, these results underscore the

complexity of biomass distribution across different forest types, highlighting the significant differences within these ecosystems.

3.5.1 Overview of Descriptive Statistics for Biomass

Metrics including mean, median, standard deviation (SD), and range provided were calculated for biomass of all three datasets: TLS All, FIA All, and Unmatched TLS. These metrics provide insights into the central tendencies and variability of biomass within each group. Figure 12 illustrates the aboveground biomass estimates from TLS All, FIA All, and Unmatched TLS divided into plots for 12A. the entire dataset for all forest types; 12B. deciduous forests at 12C. black spruce forests and 12D. mixed Forests.

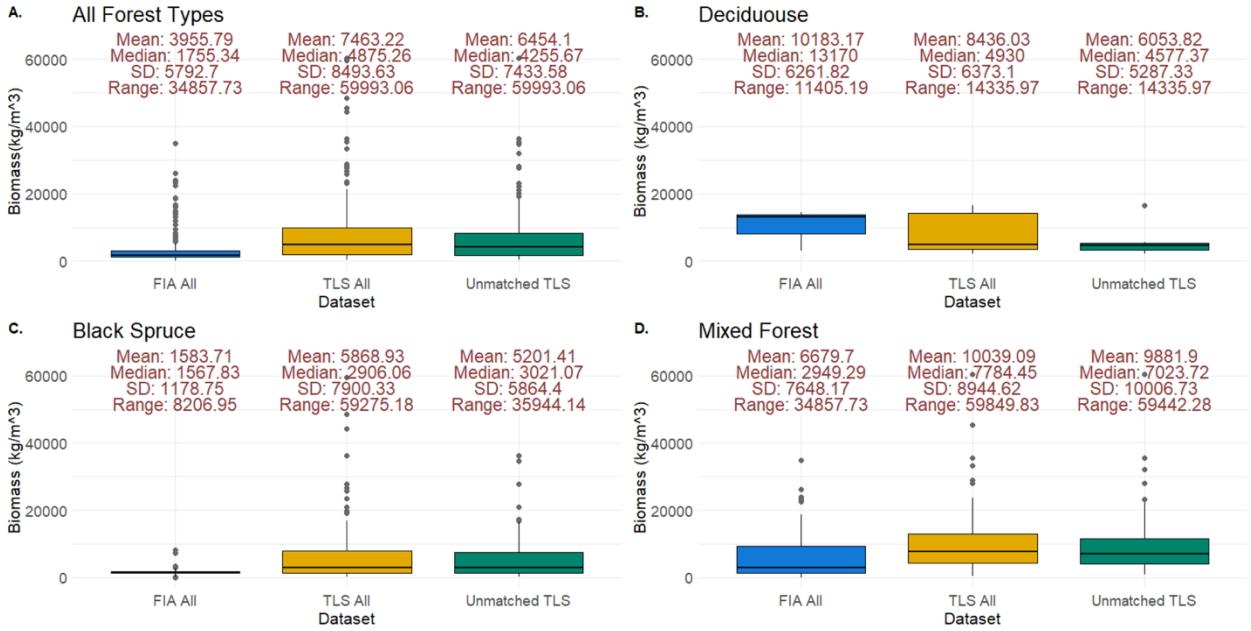

Figure 12: Boxplots comparing biomass (y) across three Datasets (x), TLS All, FIA All, and Unmatched TLS. TLS All includes all trees detected using TLS, FIA All includes all FIA recorded trees, and Unmatched TLS is a subsample of the TLS data.

3.5.1.1 Full Dataset

For the full dataset (Figure 12A), the mean biomass was highest for TLS All (7463 kg/m^3) compared to FIA All (3955 kg/m^3) and Unmatched TLS (6454 kg/m^3). This may reflect the overestimation od DBH used to calculate biomass in TLS detected trees. The median biomass for FIA All (1755 kg/m^3) was lower than that of both TLS All (4875 kg/m^3) and Unmatched TLS (4255 kg/m^3), suggesting a skewed distribution in the FIA dataset, likely driven by a few large trees contributing disproportionately to total biomass. This skey is likely due to the FIA dataset consists of mostly trees with aa DBH greater than 12.7 cm, and the trees measured on the microplot. The standard deviation was highest for TLS All (8493 kg/m^3), indicating greater variability in biomass detected by the TLS system compared to the other categories. There are two likely reasons this may occurs, first is the overestimation of DBH causes inflated biomass values, second is the limited inclusion of FIA due to measurement parameters which effects Unmatched TLS as well. Unmatched TLS contains trees that most likely do not have FIA counterparts. If FIA trees represent a limited range, Unmatched TLS represents trees outside of that range. The range for TLS All (59993 kg/m^3) was considerably larger than that for FIA All

(34857 kg/m^3) and Unmatched TLS (59993 kg/m^3) highlighting the broader spread of biomass values captured by the TLS system.

3.5.1.2 Deciduous Forests

In deciduous forests (Figure 12B), the mean biomass for FIA All (10183.17 kg/m^3) exceeded that of TLS All (8436 kg/m^3) and Unmatched TLS (6053 kg/m^3) indicating that FIA manual measurements tended to capture greater biomass on average compared to TLS scans. The median biomasses for FIA and TLS were 13170 kg/m^3 and 4930 kg/m^3 respectively. The standard deviation for FIA All (6261kg/m^3) was also high, implying significant variability in the biomass measurements. The range for FIA All (11405kg/m^3) was larger than that for TLS All (14336 kg/m^3) and Unmatched TLS (14336 kg/m^3), suggesting that manual FIA measurements captured a wider distribution of biomass values.

3.5.1.3 Black Spruce Forests

For black spruce forests (Figure 12C), the mean biomass was highest for TLS All (5869 kg/m^3), followed by Unmatched TLS (5201 kg/m^3), and lowest for FIA All (1583 kg/m^3), TLS tended to estimate a greater biomass than the FIA manual measurements in the black spruce forests. The median biomass for Unmatched TLS (3021 kg/m^3) was higher than for TLS All (2906 kg/m^3) or FIA All (1568 kg/m^3), which could indicate a positively skewed distribution for Unmatched TLS due to a few trees with particularly high biomass values. The standard deviation was the largest for TLS All (7900 kg/m^3), indicating substantial variability in biomass values measured by the TLS system. As shown in Figure 12C, black spruce forests had the most outliers compared to the other forest types, which may be attributed to the higher count of black spruce trees and their generally smaller size. One possible explanation for the larger outliers in TLS All could be incorrect classifications from the Random Forest model, which occasionally confused black spruce and white spruce. White spruce was more common in mixed forest plots. The range for TLS All (59275 kg/m^3) was significantly greater than that of FIA All (8206 kg/m^3) and Unmatched TLS (35944 kg/m^3), suggesting greater heterogeneity in biomass captured by TLS in black spruce forests.

3.5.1.4 Mixed Forests

In mixed forests (Figure 12D), the mean biomass was highest for TLS All (10039 kg/m^3), followed by FIA All (6679kg/m^3), and Unmatched TLS (9882 kg/m^3). The median biomass was lower for FIA All (2949 kg/m^3) than for TLS All (7784 kg/m^3) and Unmatched TLS (7023 kg/m^3), suggesting that TLS tended to estimate higher biomass values for mixed forests. The standard deviation was comparable for TLS All (8944 kg/m^3) and FIA All (7648 kg/m^3), indicating similar levels of variability between the two methods. The range was smaller for FIA All (34858 kg/m^3) than for TLS All (59850 kg/m^3) and Unmatched TLS (59442 kg/m^3).

3.5.2 Biomass Estimate Discrepancies and Implications

TLS consistently detected more trees than FIA, especially in black spruce plots where TLS detected numerous smaller individuals (Figure 7). The discrepancies between TLS All and FIA All in Figure 11 can be partially attributed to this difference in detection capability. Additionally, the Unmatched TLS category showed substantial biomass in black spruce plots, which is consistent with the expectation that these plots have a higher tree density and smaller tree sizes that FIA did not measure.

Analysis of total biomass across all trees (Figure 11) showed that TLS All had consistently higher biomass estimates than FIA All, particularly in black spruce forests. This result was expected, as TLS identified trees that were not measured by FIA due to FIA's criteria of only including trees with a DBH of 12.5 cm or greater. In Figure 7, it is apparent how many more trees were detected by TLS than measured by FIA. The unmatched TLS category contained missing trees from FIA, contributing significantly to total biomass, especially in black spruce plots. This highlights the limitations of the FIA protocol in measuring smaller trees. However, from the comparison of DBH and height errors between matched trees (Figure 9), it is evident that TLS overestimated biomass, with this inflation being more pronounced in mixed and black spruce forests than in deciduous forests. In deciduous forests, the lower variability in biomass estimates (Figure 9A and 11A) suggests that these forests are less prone to discrepancies between TLS and manual measurements.

Visually assessing Figure 9, it is evident that deciduous forests generally had the closest biomass estimates between TTLS All and FIA All. This suggests a higher consistency between the TLS-derived and manually measured biomass estimates for deciduous plots. In contrast, black spruce plots showed a marked difference, with TLS All exhibiting the highest biomass among the categories. This result was expected because of the higher number of trees in black spruce plots, as reflected in the tree count table, where many smaller trees were not measured by FIA because of the DBH threshold. This highlights TLS's strength in capturing smaller trees, but also underscores the need for better tree-matching methods to reduce errors caused by occlusion and dense canopies (Åkerblom and Kaitaniemi 2021; Wardius and Hein 2024; Calders et al. 2020; Boucher et al. 2021). Mixed forests showed variability, but the general trend remained consistent with other forest types: TLS All often captured more biomass, while Unmatched TLS and FIA All values varied depending on the specific plot.

3.6 Broader Ecological and Methodological Implications

TLS provides significant advantages in forest inventories by detecting smaller trees, which are critical for accurate biomass estimation in boreal forests, essential for understanding carbon dynamics (Liang et al. 2016; Wardius and Hein 2024). However, TLS's tendency to overestimate biomass in complex forest structures emphasizes the need for careful calibration (Åkerblom and Kaitaniemi 2021; Wardius and Hein 2024; Boucher et al. 2021). Accurate biomass estimates are crucial for assessing carbon stocks in boreal ecosystems, which play a key role in global carbon storage (Lim et al. 2019). The discrepancies observed in biomass estimates between TLS and FIA (Figures 9 and 10) underscore the need for improved calibration, especially in structurally complex forests, such as black spruce and mixed forests. These findings have significant implications for understanding forest carbon stocks, particularly in boreal regions, where accurate biomass assessments are vital.

4 Conclusion

TLS-based systems, such as the FARO Focus, offer significant advantages in capturing detailed forest structure and biomass, especially in dense and complex forests. However, calibration, validation, and consideration of species and forest type are necessary to minimize estimation errors, making TLS a valuable tool for improving forest inventories and carbon stock assessments. The findings of this study, including the significant discrepancies in DBH, height, and

biomass across different forest types (Figures 7, 8, 9, 10, 11, and 12), emphasize the need for species- and forest type-specific calibration to improve accuracy. Continued refinement of TLS methods, along with improved tree-matching processes and integration with other remote sensing techniques, will be crucial for ensuring reliable forest measurements and enhancing our understanding of carbon dynamics in boreal ecosystems.

4.1 Future Research

Future research should focus on integrating TLS with ALS and MLS to assess forest structure across larger scales and to improve species-specific calibration models and error correction methods to enhance biomass estimation accuracy (Liang et al. 2016; Wardius and Hein 2024; LaRue et al. 2020). Puletti et al. (2020) emphasized the utility of linking Lidar observations across different scales—from ground (TLS & MLS), to airborne (ALS), to satellite (GEDI)—to improve forest biomass estimation, supporting this study's proposal for broader integration. ALS, which captures data from above, could improve height measurement accuracy by reducing occlusion effects (Wagers et al. 2021). A study on the complementary use of TLS with MLS address limitations in dense forest environments by using TLS data as a reference with SLAM aligned MLS trajectories. By extracting virtual features from MLS, such as tree stem centerlines, and real features from point clouds. This hybrid method achieved mapping accuracy with mean errors below 2 cm, even under the challenging conditions in boreal forests, with occlusions and sparse feature distribution, demonstrating the robustness of SLAM for integrating TLS and MLS data in forest inventories (Shao et al., 2020).

This study had several key limitations that impacted the accuracy and generalizability of the findings. The tree-matching process between TLS-detected and FIA-measured trees was challenging because of positional inaccuracies, particularly in dense canopies such as black spruce forests, leading to potential misalignment and bias. Refining tree-matching methods and calibration models will help reduce errors and improve the accuracy of TLS-derived forest metrics. A more robust dataset of matched trees is key form improving the accuracy of the random forest model, especially for minority classes such as the paper birch. Species-specific limitations arose from the use of allometric equations that may not fully account for regional variations, with smaller sample sizes for species like paper birch contributing to greater errors in height and biomass estimates. Occlusion from overlapping branches also hindered TLS's ability to capture upper canopy data, further complicating measurements in dense forests. Incorporating ALS or MLS may help with decreasing occlusion from above or within the plot. TLS overestimated biomass due to errors in the DBH and height measurements used to calculate biomass. Improved automated segmentation, particularly in dense forests, would result in more accurate biomass estimates. Complex forest structures in mixed forests exhibited higher error rates, indicating that TLS is more accurate in homogeneous stands such as deciduous forests. While MLS and ALS were excluded due to being beyond the scope of this study, their integration could improve data accuracy. Lastly, the study's limited sample size and regional focus on Alaska's boreal forests reduce the generalizability of the results to other forest types and regions, underscoring the need for further research to refine methods and improve species-specific biomass estimation.

5 Work Cited

Åkerblom, Markku, and Pekka Kaitaniemi. 2021. “Terrestrial Laser Scanning: A New Standard of Forest Measuring and Modelling?” *Annals of Botany* 128 (6): 653–62. https://doi.org/10.1093/aob/mcab111.

Albrich, Katharina, Werner Rammer, Monica G. Turner, Zak Ratajczak, Kristin H. Braziunas, Winslow D. Hansen, and Rupert Seidl. 2020. “Simulating Forest Resilience: A Review.” Edited by Thomas Hickler. *Global Ecology and Biogeography* 29 (12): 2082–96. https://doi.org/10.1111/geb.13197.

Batchelor, Jonathan L., Eric Rowell, Susan Prichard, Deborah Nemens, James Cronan, Maureen C. Kennedy, and L. Monika Moskal. 2023. “Quantifying Forest Litter Fuel Moisture Content with Terrestrial Laser Scanning.” *Remote Sensing* 15 (6): 1482. https://doi.org/10.3390/rs15061482.

Batchelor, Jonathan L., Todd M. Wilson, Michael J. Olsen, and William J. Ripple. 2022. “New Structural Complexity Metrics for Forests from Single Terrestrial Lidar Scans.” *Remote Sensing* 15 (1): 145. https://doi.org/10.3390/rs15010145.

Bauwens, Sébastien, Harm Bartholomeus, Kim Calders, and Philippe Lejeune. 2016. “Forest Inventory with Terrestrial LiDAR: A Comparison of Static and Hand-Held Mobile Laser Scanning.” *Forests* 7 (12): 127. https://doi.org/10.3390/f7060127.

Blehm, James, Folwell Ave, and St Paul. 2010. “FOREST INVENTORY AND ANALYSIS.”

Boucher, Peter B, Ian Paynter, David A Orwig, Ilan Valencius, and Crystal Schaaf. 2021. “Sampling Forests with Terrestrial Laser Scanning.” *Annals of Botany* 128 (6): 689–708. https://doi.org/10.1093/aob/mcab073.

Calders, Kim, Jennifer Adams, John Armston, Harm Bartholomeus, Sebastien Bauwens, Lisa Patrick Bentley, Jerome Chave, et al. 2020. “Terrestrial Laser Scanning in Forest Ecology: Expanding the Horizon.” *Remote Sensing of Environment* 251 (December):112102. https://doi.org/10.1016/j.rse.2020.112102.

Calvin, Katherine, Dipak Dasgupta, Gerhard Krinner, Aditi Mukherji, Peter W. Thorne, Christopher Trisos, José Romero, et al. 2023. “IPCC, 2023: Climate Change 2023: Synthesis Report. Contribution of Working Groups I, II and III to the Sixth Assessment Report of the Intergovernmental Panel on Climate Change [Core Writing Team, H. Lee and J. Romero (Eds.)]. IPCC, Geneva, Switzerland.” First. Intergovernmental Panel on Climate Change (IPCC). https://doi.org/10.59327/IPCC/AR6-9789291691647.

“Campbell Tract Special Recreation Management Area.” n.d. US Department of Interior Bureau of Land Managment. https://www.blm.gov/visit/campbell-tract.

Chapin, F.S., A.D. McGuire, R.W. Ruess, T.N. Hollingsworth, M.C. Mack, J.F. Johnstone, E.S. Kasischke, et al. 2010. “Resilience of Alaska’s Boreal Forest to Climatic changeThis Article Is One of a Selection of Papers from The Dynamics of Change in Alaska’s Boreal Forests: Resilience and Vulnerability in Response to Climate Warming.” *Canadian Journal of Forest Research* 40 (7): 1360–70. https://doi.org/10.1139/X10-074.

Chi, Hong, Guoqing Sun, Jinliang Huang, Zhifeng Guo, Wenjian Ni, and Anmin Fu. 2015. “National Forest Aboveground Biomass Mapping from ICESat/GLAS Data and MODIS Imagery in China.” *Remote Sensing* 7 (5): 5534–64. https://doi.org/10.3390/rs70505534.

Chojnacky, Davd C. 2012. “FIA’s Volume-to-Biomass Conversion Method (CRM) Generally Underestimates Biomass in Comparison to Published Equations.”

“CloudCompare v2.13.Beta.” 2024. http://www.cloudcompare.org/.

Cook, Bruce, Lawrence Corp, Ross Nelson, Elizabeth Middleton, Douglas Morton, Joel McCorkel, Jeffrey Masek, Kenneth Ranson, Vuong Ly, and Paul Montesano. 2013. “NASA Goddard’s LiDAR, Hyperspectral and Thermal (G-LiHT) Airborne Imager.” *Remote Sensing* 5 (8): 4045–66. https://doi.org/10.3390/rs5084045.

Donager, Jonathon J., Andrew J. Sánchez Meador, and Ryan C. Blackburn. 2021. “Adjudicating Perspectives on Forest Structure: How Do Airborne, Terrestrial, and Mobile Lidar-Derived Estimates Compare?” *Remote Sensing* 13 (12): 2297. https://doi.org/10.3390/rs13122297.

Dunn, O. J. 1964. “Multiple Comparisons Using Rank Sums.” *Technometrics* 6 (3): 241–52.

“FIELD INSTRUCTIONS FOR THE ANNUAL INVENTORY OF ALASKA.” 2020. FOREST INVENTORY AND ANALYSIS RESOURCE MONITORING AND ASSESSMENT PROGRAM PACIFIC NORTHWEST RESEARCH STATION USDA FOREST SERVICE.

“Focus Premium and Focus Core User Documentation.” 2022. FARO Technologies Inc. https://downloads.faro.com/index.php/apps/files_pdfviewer/?file=...es%3D08M85E00_FARO_Focus_Premium-Core_Laser_Scanner_2022Oct.pdf.

Heidenreich, Marius G., and Dominik Seidel. 2022. “Assessing Forest Vitality and Forest Structure Using 3D Data: A Case Study From the Hainich National Park, Germany.” *Frontiers in Forests and Global Change* 5 (June):929106. https://doi.org/10.3389/ffgc.2022.929106.

Hessburg, Paul F., Carol L. Miller, Sean A. Parks, Nicholas A. Povak, Alan H. Taylor, Philip E. Higuera, Susan J. Prichard, et al. 2019. “Climate, Environment, and Disturbance History Govern Resilience of Western North American Forests.” *Frontiers in Ecology and Evolution* 7 (July):239. https://doi.org/10.3389/fevo.2019.00239.

Hudak, Andrew T, Patrick A Fekety, Van R Kane, Robert E Kennedy, Steven K Filippelli, Michael J Falkowski, Wade T Tinkham, et al. 2020. “A Carbon Monitoring System for Mapping Regional, Annual Aboveground Biomass across the Northwestern USA.” *Environmental Research Letters* 15 (9): 095003. https://doi.org/10.1088/1748-9326/ab93f9.

Hyyppä, Juha, Anttoni Jaakkola, Yuwei Chen, Antero Kukko, Harri Kaartinen, Lingli Zhu, Petteri Alho, and Hannu Hyyppä. 2013. “Unconventional LIDAR Mapping from Air, Terrestrial and Mobile.” *Photogrammetric Week*.

Jones, Miriam C., Guido Grosse, Claire Treat, Merritt Turetsky, Katey Walter Anthony, and Laura Brosius. 2023. “Past Permafrost Dynamics Can Inform Future Permafrost Carbon-Climate Feedbacks.” *Communications Earth & Environment* 4 (1): 272. https://doi.org/10.1038/s43247-023-00886-3.

Jorgenson, M. Torre, Vladimir Romanovsky, Jennifer Harden, Yuri Shur, Jonathan O’Donnell, Edward A. G. Schuur, Mikhail Kanevskiy, and Sergei Marchenko. 2010. “Resilience and Vulnerability of Permafrost to Climate changeThis Article Is One of a Selection of Papers from The Dynamics of Change in Alaska’s Boreal Forests: Resilience and Vulnerability in Response to Climate Warming.” *Canadian Journal of Forest Research* 40 (7): 1219–36. https://doi.org/10.1139/X10-060.

Kendall, M G. n.d. “A NEW MEASURE OF RANK CORRELATION.”

Kodors, Sergejs. 2017. “Point Distribution as True Quality of LiDAR Point Cloud.” *Baltic Journal of Modern Computing* 5 (4). https://doi.org/10.22364/bjmc.2017.5.4.03.

Kruskal and Wallis. 1952. “Use of Ranks in One-Criterion Variance Analysis.” *Journal of the American Statistical Association* 47:583–621.

Kükenbrink, Daniel, Mauro Marty, Ruedi Bösch, and Christian Ginzler. 2022. “Benchmarking Laser Scanning and Terrestrial Photogrammetry to Extract Forest Inventory Parameters in a Complex Temperate Forest.” *International Journal of Applied Earth Observation and Geoinformation* 113 (September):102999. https://doi.org/10.1016/j.jag.2022.102999.

Kukko, Antero, Risto Kaijaluoto, Harri Kaartinen, Ville V. Lehtola, Anttoni Jaakkola, and Juha Hyyppä. 2017. “Graph SLAM Correction for Single Scanner MLS Forest Data under Boreal Forest Canopy.” *ISPRS Journal of Photogrammetry and Remote Sensing* 132 (October):199–209. https://doi.org/10.1016/j.isprsjprs.2017.09.006.

LaRue, Elizabeth, Franklin Wagner, Songlin Fei, Jeff Atkins, Robert Fahey, Christopher Gough, and Brady Hardiman. 2020. “Compatibility of Aerial and Terrestrial LiDAR for Quantifying Forest Structural Diversity.” *Remote Sensing* 12 (9): 1407. https://doi.org/10.3390/rs12091407.

“Leica BLK2GO User Manual Version 0.9.” n.d. Leica Geosystems.

“Leica BLK360 User Manual Version 4.0.” n.d. Leica Geosystems.

Liang, Xinlian, Ville Kankare, Juha Hyyppä, Yunsheng Wang, Antero Kukko, Henrik Haggrén, Xiaowei Yu, et al. 2016. “Terrestrial Laser Scanning in Forest Inventories.” *ISPRS Journal of Photogrammetry and Remote Sensing* 115 (May):63–77. https://doi.org/10.1016/j.isprsjprs.2016.01.006.

Lim, Hyungwoo, Ram Oren, Torgny Näsholm, Monika Strömgren, Tomas Lundmark, Harald Grip, and Sune Linder. 2019. “Boreal Forest Biomass Accumulation Is Not Increased by Two Decades of Soil Warming.” *Nature Climate Change* 9 (1): 49–52. https://doi.org/10.1038/s41558-018-0373-9.

Liu, Guancheng, Guoyong Yan, Mengyu Chang, Binbin Huang, Xingyu Sun, Shijie Han, Yajuan Xing, and Qinggui Wang. 2021. “Long-Term Nitrogen Addition Further Increased Carbon Sequestration in a Boreal Forest.” *European Journal of Forest Research* 140 (5): 1113–26. https://doi.org/10.1007/s10342-021-01386-9.

Montesano, P.M., R.F. Nelson, R.O. Dubayah, G. Sun, B.D. Cook, K.J.R. Ranson, E. Næsset, and V. Kharuk. 2014. “The Uncertainty of Biomass Estimates from LiDAR and SAR across a Boreal Forest Structure Gradient.” *Remote Sensing of Environment* 154 (November):398–407. https://doi.org/10.1016/j.rse.2014.01.027.

Nitze, I., G. Grosse, B. M. Jones, V. E. Romanovsky, and J. Boike. 2018. “Remote Sensing Quantifies Widespread Abundance of Permafrost Region Disturbances across the Arctic and Subarctic.” *Nature Communications* 9 (1): 5423. https://doi.org/10.1038/s41467-018-07663-3.

Nowacki, G, and T Brock. 1995. “Ecoregions and Subregions of Alaska.”

Persson, Henrik J., Kenneth Olofsson, and Johan Holmgren. 2022. “Two-Phase Forest Inventory Using Very-High-Resolution Laser Scanning.” *Remote Sensing of Environment* 271 (March):112909. https://doi.org/10.1016/j.rse.2022.112909.

Petras, Vaclav, Anna Petrasova, James B. McCarter, Helena Mitasova, and Ross K. Meentemeyer. 2023. “Point Density Variations in Airborne Lidar Point Clouds.” *Sensors* 23 (3): 1593. https://doi.org/10.3390/s23031593.

Puletti, Nicola, Mirko Grotti, Carlotta Ferrara, and Francesco Chianucci. 2020. “Lidar-Based Estimates of Aboveground Biomass through Ground, Aerial, and Satellite Observation: A Case Study in a Mediterranean Forest.” *Journal of Applied Remote Sensing* 14 (4): 044501. https://doi.org/10.1117/1.JRS.14.044501.

Puletti, Nicola, Mirko Grotti, Carlotta Ferrara, and Stefano Scalercio. 2021. “Traditional and TLS-Based Forest Inventories of Beech and Pine Forests Located in Sila National Park: A Dataset.” *Data in Brief* 34 (February):106617. https://doi.org/10.1016/j.dib.2020.106617.

R Core Team. 2024. “R Studio.”

Rantanen, Mika, Alexey Karpechko, Antti Lipponen, Kalle Nordling, Otto Hyvärinen, Kimmo Ruosteenoja, Timo Vihma, and Ari Laaksonen. 2021. “The Arctic Has Warmed Four Times Faster than the Globe since 1980.” Preprint. In Review. https://doi.org/10.21203/rs.3.rs-654081/v1.

Richardson, Jeffrey J, and L. Monika Moskal. 2014. “Uncertainty in Urban Forest Canopy Assessment: Lessons from Seattle, WA, USA.” *Urban Forestry & Urban Greening* 13 (1): 152–57. https://doi.org/10.1016/j.ufug.2013.07.003.

Roussel, Jean-Romain, David Auty, Nicholas C. Coops, Piotr Tompalski, Tristan R.H. Goodbody, Andrew Sánchez Meador, Jean-François Bourdon, Florian De Boissieu, and Alexis Achim. 2020. “lidR: An R Package for Analysis of Airborne Laser Scanning (ALS) Data.” *Remote Sensing of Environment* 251 (December):112061. https://doi.org/10.1016/j.rse.2020.112061.

Sánchez Meador, Andrew, J. Donager, and Jeffery B Cannon. 2022. “Spanner.” https://github.com/bi0m3trics/spanner.

“SCENE.” 2019. FARO.

Schulz, Beth. 2014. “US Forest Service Forest Inventory and Analysis Program (FIA).”

Shao, Jie, Wuming Zhang, Nicolas Mellado, Nan Wang, Shuangna Jin, Shangshu Cai, Lei Luo, Thibault Lejemble, and Guangjian Yan. 2020. “SLAM-Aided Forest Plot Mapping Combining Terrestrial and Mobile Laser Scanning.” *ISPRS Journal of Photogrammetry and Remote Sensing* 163 (May):214–30. https://doi.org/10.1016/j.isprsjprs.2020.03.008.

“Study Sites & Design: Bonanza Creek Experimental Forest.” 2002. Bonanza Creek LTER. 2002.

Terryn, Louise, Kim Calders, Markku Åkerblom, Harm Bartholomeus, Mathias Disney, Shaun Levick, Niall Origo, Pasi Raumonen, and Hans Verbeeck. 2023. “Analysing Individual 3D Tree Structure Using the R Package ITSMe.” *Methods in Ecology and Evolution* 14 (1): 231–41. https://doi.org/10.1111/2041-210X.14026.

Terryn, Louise, Kim Calders, Mathias Disney, Niall Origo, Yadvinder Malhi, Glenn Newnham, Pasi Raumonen, Markku Å Kerblom, and Hans Verbeeck. 2020. “Tree Species Classification Using Structural Features Derived from Terrestrial Laser Scanning.” *ISPRS Journal of Photogrammetry and Remote Sensing* 168 (October):170–81. https://doi.org/10.1016/j.isprsjprs.2020.08.009.

Thompson, Ian D., ed. 2009. *Forest Resilience, Biodiversity, and Climate Change: A Synthesis of the Biodiversity / Resiliende / Stability Relationship in Forest Ecosystems*. CBD Technical Series 43. Montreal: Secretariat of the Convention on Biological Diversity.

Vorster, Anthony G., Paul H. Evangelista, Atticus E. L. Stovall, and Seth Ex. 2020. "Variability and Uncertainty in Forest Biomass Estimates from the Tree to Landscape Scale: The Role of Allometric Equations." *Carbon Balance and Management* 15 (1): 8. https://doi.org/10.1186/s13021-020-00143-6.

Wagers, Steven, Guillermo Castilla, Michelle Filiatrault, and G. Arturo Sanchez-Azofeifa. 2021. "Using TLS-Measured Tree Attributes to Estimate Aboveground Biomass in Small Black Spruce Trees." *Forests* 12 (11): 1521. https://doi.org/10.3390/f12111521.

Wardius, Yannik, and Sebastian Hein. 2024. "Terrestrial Laser Scanning vs. Manual Methods for Assessing Complex Forest Stand Structure: A Comparative Analysis on Plenter Forests." *European Journal of Forest Research* 143 (2): 635–49. https://doi.org/10.1007/s10342-023-01641-1.

Webb, James, and Parker Solar. n.d. "Open Science at NASA." https://science.nasa.gov/open-science/.

Weldon, James, and Ulf Grandin. 2019. "Major Disturbances Test Resilience at a Long-term Boreal Forest Monitoring Site." *Ecology and Evolution* 9 (7): 4275–88. https://doi.org/10.1002/ece3.5061.

Wilcoxon, F. 1945. "Individual Comparisons by Ranking Methods." *Biometrics Bulletin* 1 (6).

Wirth, C., J. W. Lichstein, J. Dushoff, A. Chen, and F. S. Chapin. 2008. "WHITE SPRUCE MEETS BLACK SPRUCE: DISPERSAL, POSTFIRE ESTABLISHMENT, AND GROWTH IN A WARMING CLIMATE." *Ecological Monographs* 78 (4): 489–505. https://doi.org/10.1890/07-0074.1.

Yrttimaa, Tuomas, Ville Luoma, Ninni Saarinen, Ville Kankare, Samuli Junttila, Markus Holopainen, Juha Hyyppä, and Mikko Vastaranta. 2020. "Structural Changes in Boreal Forests Can Be Quantified Using Terrestrial Laser Scanning." *Remote Sensing* 12 (17): 2672. https://doi.org/10.3390/rs12172672.

"ZEB-HORIZON User Manual v1.3." 2020. GeoSLAM Ltd.

6 Acknowledgments

I (Rachel Deininger) am the primary developer of the science document. Dr. L. Monika Moskal (Professor at the University of Washington) is my primary advisor and my committee chair. Hans Erik-Andersen and Jonathan L Batchelor are Committee members. Anthony Stewart and Hannah Redford assisted in collecting MLS and TLS scans in the field. I would also like to acknowledge the employees at Alaska Division of Natural Resources and Anchorage Forestry Science Lab who aided in the field data collection. I would like to acknowledge the Bridging the Gap Fellowship and US Forest Service for funding this project and the support of the Precision Forestry Cooperative and Remote Sensing and Geospatial Analysis Lab at the University of Washington.

7 Appendix A. Field Guide

7.1 Introduction

This field work will help the development of sampling techniques using terrestrial Lidar scanners, applying a combination of terrestrial and airborne Lidar and manual sampling methods. The field work takes place in Alaskan boreal forests outside of Anchorage and Fairbanks in the summers between 2022 and 2024. The objective is to accurately determine forest biometrics such as aboveground biomass with fine scale terrestrial scanning and scale it up to airborne scanning to increase the accuracy and potential of large-scale airborne scans in boreal forests. The Forest inventory Analysis (FIA) program in Alaska and more broadly the US Forest Service will benefit from this project. The sampling sites will be on preexisting FIA plots, which are manually sampled on a ten-year basis. Not only will this study be beneficial for the parties involved but for a range of scientists seeking to better understand how Lidar technologies can be used to assess and measure forest variables. This work will help push the boundaries of what Lidar technology can be used for providing insight into the shortcomings and strengths of terrestrial Lidar technology. Companies developing Lidar technology will be able to learn from the performance of different scanners in the novel boreal forest environment. The first stage of this project will compare multiple scanners in their usability in the field and how they handle dense vegetation.

This Field Guide will do the following:

- Introduce the project's designee and purpose.
- Familiarize uses with the location of data collection
- Detail the safety guidelines that must be followed in the field
- Instruct field personnel in locating and setting up field plots.
- Instruct field personnel in the use of four terrestrial laser scanners, two of which are mobile.
- Detail the process of downloading data from different scanners.

7.2 Project description

7.2.1 Study Areas

The study areas for this project are near Anchorage and Fairbanks Alaska.

7.2.1.1 Anchorage

Campbell Tract Special Recreation Management Area

The initial sampling strategy was tested in Campbell Tract Special Recreation Management Area (CTSRMA) adjoined to Far North Bicentennial Park in Anchorage Alaska over a period of two weeks between September 12th, 2022, and September 23rd, 2022. Campbell Tract seen in Figure 2 is a Bureau of Land Management owned recreation area with 730 acres of forest (BLM). This location was chosen for its easy accessibility and close proximity to Anchorage, similar forests characteristics to interior Alaska, and field measurements taken manually by FIA crews are available for the established plots.

7.2.1.2 Fairbanks

Bonanza Creek Experimental Forest and Caribou-Poker Creek Research Watershed

The second phase of sampling was in Bonanza Creek Experimental Forest (BCEF) outside of Fairbank Alaska for six-weeks between June and August 2023. These sites were chosen for their accessibility from the city of Fairbanks, the presence of pre-established FIA plots, and the ecological gradient across the parks is archetypal of interior Alaska's boreal forests (UFA). Throughout the Yukon River watershed and around Fairbanks the ecoregions are classified as Interior Alaskan-Yukon Lowland Taiga and Yukon Interion Dry Forest (Margolis et al. 2015). At the CPCRW, there are statistically sufficient field plots and Airborne scans to represent interior Alaska's boreal forests allowing us to apply small sized sampling to a regional scale. A 2024 summer field season to sample Caribou-Poker Creek Research Watershed (CPCRW) just outside of Fairbanks is in the planning stage.

7.2.2 Units of measurement

English Units will be used unless otherwise specified

7.3 Literature Review

7.3.1 Boreal Forests

Boreal forests provide many ecosystem functions, they act as an important sink for carbon with soils containing the largest global organic carbon pool (Lim et al. 2019, Margolis et al. 2015). These forest account for 30% of earth's forested area and 14.5% of the total land area on earth (Liu eta al. 2021). They are also at high risk from climate change. Hotter days and longer droughts stress the trees and make them more susceptible to insect infestations and infections. Increasing temperatures can also cause a positive feedback loop in the boreal regions. As soil temperature rises, decomposition increases releasing more carbon into the atmosphere (Lim et al. 2019).

Boreal Forests are nitrogen limited due to their temperature constraints restricting nitrogen mineralization. However, the increasing decomposition of organic matter in northern soils from higher temperatures can create more bioavailable nitrogen. In theory reducing the strain of limited nitrogen allows for increased vegetation growth resulting in carbon sequestration (Lim et al. 2019). However, the question remains would this increased growth last over an extended period of time and is it enough to offset carbon emissions from increased decomposition in the soils.

7.3.2 Remote Sensing Lidar

Remote sensing has been used to study many ecological properties such as landscape, vegetation stress, and biometrics. It is a fast non-intrusive method for studying the surface of the earth. Remote sensing can be performed both passively, optical, or actively, radar and Lidar. Optical has the highest quantity of available data, especially satellite data which had been collected consistently since 1972 using NASA's Landsat satellites (Vorster et al, 2020).

In remote sensing, Lidar (Light Detection and Ranging), is an active remote sensing method that uses lasers to measure distance. Time of flight Lidar scanners sends out a pulse, which hits an object and returns to the scanner. The distance the pulse traveled is measured based on how long it took the pulse to return, and a point is created for the location the pulse hit (Bauwenset al, 2016). The compilation of all these points creates a point cloud, which has a variety of uses such as in autonomous car ecosystems, aiding the visually impaired, and mapping

forest structure (Hyyppä et al, 2013). Lidar can be used to calculate forest structure variables such as stem maps, canopy height, above ground biomass, and diameter at breast height (Heidenreich and Seidel, 2022; Quio et al, 2023). Lidar can be used to measure the effect of stressors on the vitality of forest based on their changing structure over time (Heidenreich and Seidel, 2022). Forest structural diversity is a critical driver in forest function, it can be used to predict microclimates, hydrology, and resilience (LaRue et al, 2020). Lidar currently has limited spatial and temporal coverage, although it has been shown to be the most accurate remote sensing method for estimating stand structure attributes making it the optimal choice for conducting forest inventories (Vorster et al, 2020; Hudak et al, 2020). There are several platforms that Lidar scanners can be operated from, these include spaceborne, airborne, or terrestrial (Bauwenset al, 2016).

Terrestrial Laser Scanning (TLS) is a ground-based mechanism for collecting Lidar scans. Unlike airborne laser scanning (ALS), which is mounted to an aircraft, TLS is collected from ground level scanners wither attached to tripods, backpacks, vehicles, or handheld. ALS has the benefit of being able to cover a large area rapidly, while TLS has the benefit of finer details and more precise individual tree measurements. TLS is a phase-shift Lidar device, it emits a continuous, modulated laser beam and calculates distance by measuring the phase difference between the outgoing and returning light wave. This allows for fast, high-resolution scans at close range, though it limits effective range and prevents multiple returns from a single pulse. In contrast, time-of-flight Lidar, like ALS, emits discrete pulses and measures the time each pulse takes to return. This approach enables longer-range scanning with the capability of capturing multiple returns, making it ideal for capturing complex structures, such as forest canopies. A study of compatibility between ALS and TLS in quantifying forest structure by LaRue et al, in 2020, found strong univariate agreement in the two devices between openness, canopy height, internal heterogeneity, and leaf area. They found far less agreement in quantifying the outermost layer of the canopy, TLS devices which see the canopy from below experience a level of occlusion due to foliage (LaRue et al, 2020). One of the main downsides of TLS devices is the occlusion effect. To create a point cloud without occlusion, multiple scans must be taken throughout the plot and stitched together in post processing, making the scanning and data processing more time consuming. (Hyyppä et al. 2013; Bauwenset al, 2016).

Mobile Laser Scanning (MLS) is a type of TLS collected using a hand-held, backpack or vehicle mounted, device that an operator walks through an area (Hyyppä et al. 2013; Bauwenset al, 2016). The vehicle mounted, MLS system combines the laser scanner with a Global Navigation Satellite System (GNSS) and an inertial measurement unit (IMU), like that of the ALS system. All the components must be working and synchronized to create a quality scan. For a handheld device, GNSS is unnecessary (Bauwenset al, 2016). Less time is required to collect data and process it when using the MLS device rather than the tripod mounted TLS. TLS devices generally create a more accurate and robust point cloud, but what they gain in detail they lack in time efficiency and maneuverability. In Bauwenset al study on Lidar in Forest Inventory, they found handheld MLS scanners had a faster acquisition time and better tree detection rate than both multi and single scan TLS. For work in remote location and for forest inventory variables, MLS devices are preferable for their portability and efficiency (Kükenbrink et al. 2022). The first documented use of MLS in forestry began in early 2010 with car mounted scanners in urban areas (Bauwenset al, 2016). Since then, it has developed into a tool for forest inventory analysis.

7.3.3 Above Ground Biomass

Biomass is the amount of living matter in each habitat, it is measures as the weight of organisms per unit area (Lin et al. 2010). Above Ground Biomass (ABG), a measurement of forest structure, has a variety of uses such as estimations are a biophysical parameter that can be used to assess tree health, energy conservation, biological balance and forest regeneration (Montesano et al, 2014; Lin et al. 2010). Monitoring forest biomass over time allows disturbances such as from storms, fire, drought, or insect infestation to be tracked, along with examining forest carbon strategies and developing forest management strategies (Kankare et al, 2013; Vorster et al, 2020).

Originally biomass was measured using destructive weighting, a ground-based method. It has advanced to using all forms of remote sensing. While it is possible to measure AGB using coarse- or medium-resolution satellite imagery the estimates are often pore, especially at a local level (Kankare et al, 2013). Optical sensing often has issues with underestimation or saturation in high biomass areas since it relies on canopy closure for its calculations (Vorster et al, 2020). In a review of remote sensing methods, Dengsheng Lu found that optical and radar were better suited for estimating biomass in simple stand structure rather than complex systems (Lu, 2005). In forestry an allometric equation establishes a relationship between a key characteristic and another property. For biomass this is commonly done using diameter at breast height (DBH) and height (Vorster et al, 2020; Wagers et al, 2021; Qiao et al, 2023). Many general Allometric equations have been developed that are used for large scale biomass estimations. However, allometric equations are frequently applied to populations of trees which were not developed for leading to significant estimation errors in determining biomass. Allometric relationships vary across species, soil type, climate, and available nutrients among other environmental and geographic differences (Vorster et al, 2020). While locally developed equations can be accurate, they are difficult to apply to a large range. Calibrating equations to each species is often expensive and requires the destructive harvesting of hundreds of trees (Wagers et al, 2021). Manual data collection is the most time consuming, expensive, and labor-intensive part of any forest inventory process (Vatandaşlar and Mustafa, 2020).

Lidar can be used to calibrate allometric equations by collecting accurate forest structure and height data (Vorster et al, 2020). ALS scans can cover a wider range but have the downside of having a point density of 1 to 10 per m2 (Wagers et al, 2021). On the other hand, TLS and MLS scans have a much higher point density but don’t cover as wide a range making them ideal for calibration, where accurate forest biometrics are necessary for developing regional Allometric equations.

Anthropogenic climate change creates a caveat for traditional forest management which relies on the expectation that conditions remain constant. Modeling forests in the future must take into account a degree of variability and uncertainty in variables such as precipitation patterns, temperature, natural disasters, and other climate extremes (Heidenreich and Seidel, 2022). These variables shape their environment, influencing tree growth, forest regeneration and structure, terrain, and many other important metrics. It is possible to analyze the effects of clime change by looking at forest structural development over time (Montesano et al, 2014; Heidenreich and Seidel, 2022).

7.4 Field Safety

7.4.1 General

Workdays are long and require constant vigilance of your surroundings (keeping your eyes and ears open for dangerous wildlife in the area).

Hiking with maximum of 30 lb. of gear

7.4.2 No Go Criteria

No go if there is potentially dangerous wildfire or thunderstorms in the area, if AQI is above safe levels (150+), or temperature is above 100 degrees.

7.4.2.1 Wildfire Risk

Field crew will have a radio connected with Alaskan DNR office to stay up to date with where wildfires have spread in the area and if any have started nearby while in the field.

7.4.2.2 Thunderstorms

Thunderstorms can be determined by watching weather maps and checking the skies for signs of lightning.

Heavy rainfall or winds will also make collecting scans impossible, preventing field work. Flooding, or potential for flooding, should be noted and avoided.

7.4.2.3 High AQI

Determine if there is harmful AQI (150+) exposure for the work area using the EPA's Air Quality Index (AQI) and PurpleAir Sensor Map. The Alaska Smoke Forecast website can also be a useful planning tool when looking at longer-term planning for wildfire smoke.

7.4.3 Dangerous Wildlife

7.4.3.1 Moose

- Be aware that moose can act aggressively under certain circumstances (they feel threatened, cow feels its calf is threatened, previously stressed, etc).
- Be aware of signs moose demonstrate when stressed (long hairs on hump raised, ears laid back, licking lips).
- Back away from a stressed moose.
- Do not get between a cow moose and haircalf.
- Be aware that moose do not have predatory instincts therefore running away from a moose may be a good way of diffusing a tense situation.
- If encounter moose give them the right of way.
- If moose charges seek a barrier between yourself and the moose, this can be a clump of trees, large tress, or boulder.
- If knocked down, stay down and curl up into a ball and don't move. Protect your head with your arms and hands.
- Beware that moose can kick with all four feet.

7.4.3.2 Grizzly & Black Bear

- Attend mandatory bear behavior training prior going into the field.
- Watch then provided bear awareness training video.
- Discuss and address ongoing or new safety concerns during regularly scheduled morning briefings. discuss any bear encounter, the circumstances leading up to it, and any advice or information that was learned from the encounter.

- Learn to recognize types of bears and bear signs.
- Learn to recognize different types of encounters (curious, defensive, predatory).
- Learn personal behaviors to implement given different types of encounters and different species of bear.
- When working or traveling in potential bear habitat, every field crew will carry bear repellent spray and be familiar with their safe and effective use.
- Reduce chances of surprise bear encounters by making noise and traveling through open areas.
- If a bear is spotted in the distance, stay alert and observe the bear's activity and direction of travel.
- Beware that human voices and work noises carry long distances and may attract a curious bear. remain alert at all times
- Travel and work as a group.
- Never work alone without prior written approval from first line officer (team leader).
- In any case where a workg/m————————————————roup must split up (ie. one employee travels to a separate sub-plot) both parties must have in their possession at least one deterrent (an approved firearm or bear spray).
- When possible, avoid following game trails, especially through dense brush.
- If any member of the group feels threatened by a bear in the area, inform dispatch or local flight follower of the situation and arrange for an immediate pick-up.

7.4.4 Driving on Remote/Unpaved/Unimproved Roads

7.4.4.1 Accident Procedure

Follow car rental agency accident guidelines.

Call the local police and complete an accident report.

Contact UW Risk Services for liability exposures (property damage or bodily injury to other party or parties) exceeding rental / personal auto insurance.

7.4.4.2 Truck & Large Vehicle

- Reduce the chance for mechanical problems by checking motor and transmission oil levels, windshield wipers and fluid level, headlights, brake lights, signal lights, horn, tire pressure, and wheel lug-nuts for snugness before each trip.
- Check that your vehicle has a spare tire, tire lug-nut wrench, and jack, three triangular warning reflectors, First Aid kit, shovel, jumper cables, tow cable, fire extinguisher, tool kit and short boards when using hydraulic jack on uneven or soft ground.
- When emergency parking, be careful to exit the vehicle safely, watch for other traffic, park as far off the road as possible.
- When jump-starting a disabled vehicle, use the following sequence:
    - Clamp positive (red) end of cable to positive (+) terminal on disabled vehicle.
    - Clamp positive (red) end of cable to positive (+) terminal on good battery.
    - Clamp negative (black) end of cable to the negative (-) terminal on good battery.
    - Clamp negative (black) loose end of cable to disabled vehicle's engine block, away from battery.

    - Start the vehicle with a good battery and let it run for several minutes.
    - Start disabled vehicle and let both vehicles idle for several minutes.
    - Remove cables in reverse order they were connected.
- Lock vehicle when left unattended.
- Do not keep valuables in plain sight.
- Park in designated areas whenever possible.

7.4.4.3 Boat

- Weather forecasts and high water or flood warnings will be monitored and heeded for river systems. (Alaska River Forecast Center- http://aprfc.arh.noaa.gov/index_rivs.php).
- Crews will check weather updates throughout the day using weather channels on the radio or a call to Dispatch or a supervisor.
- Sufficient rain gear and extra layers will be carried regardless of the weather forecast.
- Rivers forecasted to be at flood stage during a trip will not be utilized (backup plans will be developed for hiking out or other forms of egress).
- A type III PFD will be worn by all trip members while on/in the water and during boat trips.
- If thrown from a boat in moving water, float on back downstream with legs in front of the body.
- Make your way to shore when possible.
- Do not stand up until near the shoreline in shallow water.
- Trip partners will assist with rescue as well as retrieving boats, paddles and any other lost equipment.

7.4.4.4 ATV

- Complete online training course (ATV RiderCourse from ATV Safety Institute- https://atvsafety.org/atv-ecourse/)
- Complete in person ATV training at beginning of field season
- Training certificates are on file with project PI: L. Monika Moskal

7.4.5 Important Contacts

Table 2: Emergency Contact Information

Name	Organization	Email	Phone
Miho Welton	Alaska Division of Forestry	miho.welton@alaska.gov	(907) 371-6562
Teresa Rose	Division of Forestry Dispatch Center Manager	teresa.rose@alaska.gov	(907) 451-2623
L. Monika Moskal	Professor at UW	lmmoskal@uw.edu	(206) 225-1510
Hans Andersen	Research Forester USFS	hans.andersen@usda.gov	(206) 747-1979
Crew Contact			
Rachel Deininger	Graduate Student at UW	rdeinin@uw.edu	(919) 548-8900
Hannah Redford	Graduate Student at UW	hredford@uw.edu	(913) 553-0705

7.5 Data

7.5.1 Plot Navigation and Installation

Plots are navigated to using Garmin and Avanza maps. Once in the area the field tecs search for signs of a plot. This can be pins, witness trees, or leftover flagging from past field seasons.

7.5.2 FIA (3)

Lead by US Forest Service, Forest Inventory Analysis (FIA) program is a nationwide inventory of all forested lands (>10% forest coverage). Data from FIA is used to estimate forest area by forest type and stand size, tree statistics by species and size, the health of the forest, and monitor change over time. Alaskan FIA varies from the lower 48 by having a lower sample intensity with one plot every 30,000 acres. Interior Alaska FIA also utilizes remote sensing in the form of Lidar, hyperspectral, thermal, and fine scale RGB.

7.5.2.1 Plot Arrangement

Plots are a circle broken up into four subplots. Subplots are 48 ft diameter circles spaced evenly apart with one at plot center, two is directly north, three is to the southeast, and four is to the southwest (Figure 1). The subplot center of each subplot is 120 ft away from the plot center.

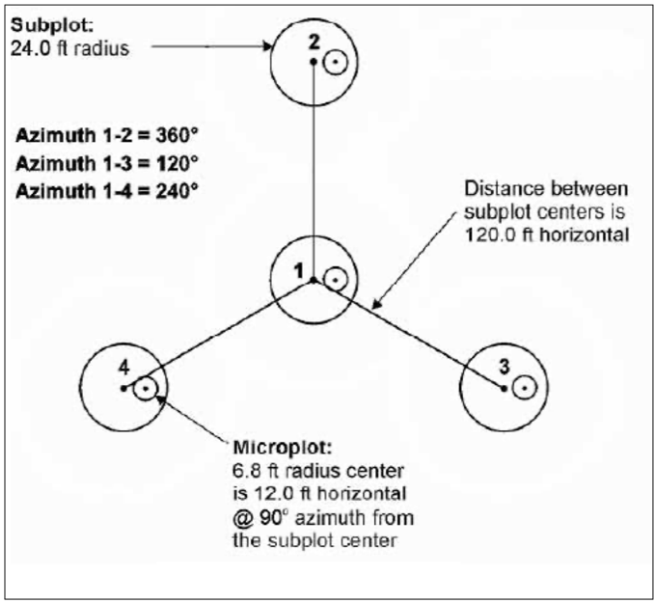

Figure 13: FIA Plot Arrangement

7.5.2.2 Pins

Sub plots are outfitted with pins to visually mark locations making them easier for field technicians to find and survey. The pins are plastic, about two feet long, and come in three different colors white, yellow, and red (Figure 14 A. D.). For each subplot there is a single white pin at the center, two yellow pins 12 ft east and west from the center, and four red pins radiating out in the woody transect lines which vary from subplots 1 through 4. For the purpose of this study the pins were only used for locating the subplots centers.

7.5.2.3 Witness Trees

Witness trees are chosen for each subplot so the center can be relocated if the pins get removed or destroyed in the 10 years between visits. They are tagged with yellow circles or silver

diamonds made of metal and nailed to the tree oriented towards subplot center (Figure 14 C. D.). Sometimes witness trees are marked with only a nail. The distance between the tree marker and the subplot center and azimuth are recorded by FIA.

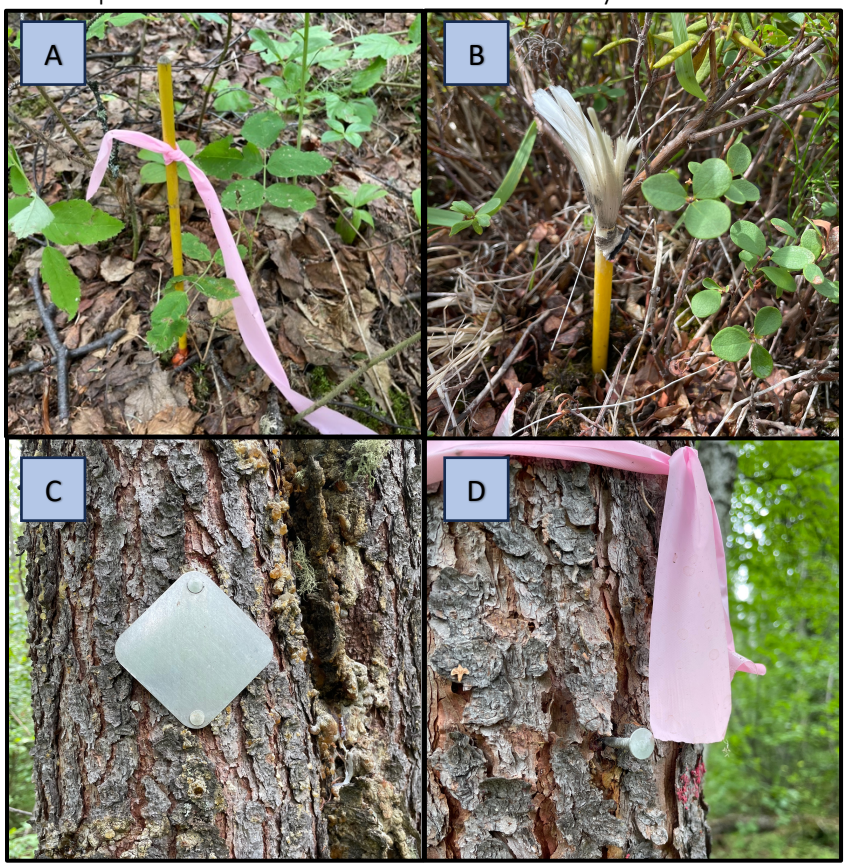

Figure 14: Pins and Witness Trees. A and B show pins used to mark the location of FIA plots. B is an example of a pin damaged in a fire. C and D show different markers used on witness trees, while C has a plaque, D is only just a nail. These are all examples of permanent monumentation used by FIA to set up and re measure plots. Photos taken by Rachel Deininger

7.5.2.4 FIA Species Codes

Tree species is recorded in the FIA field survey as a species code. The Species codes for trees native to Alaska are listed in Table 2.

Woodland	FIA Code	PLANTS Code	Common name	Genus	Species
	0011	ABAM	Pacific silver fir	*Abies*	*amabilis*
	0019	ABLA	subalpine fir	*Abies*	*lasiocarpa*
	0042	CUNO	Alaska yellow-cedar	*Cupressus*	*nootkatensis*
	0071	LALA	tamarack (native)	*Larix*	*laricina*
	0094	PIGL	white spruce	*Picea*	*glauca*
	0095	PIMA	black spruce	*Picea*	*mariana*
	0098	PISI	Sitka spruce	*Picea*	*sitchensis*
	0108	PICO	lodgepole pine	*Pinus*	*contorta*
	0231	TABR2	Pacific yew	*Taxus*	*brevifolia*
	0242	THPL	western redcedar	*Thuja*	*plicata*
	0263	TSHE	western hemlock	*Tsuga*	*heterophylla*
	0264	TSME	mountain hemlock	*Tsuga*	*mertensiana*
	0351	ALRU2	red alder	*Alnus*	*rubra*
	0375	BEPA	paper birch	*Betula*	*papyrifera*
	0376	BENE4	Alaska paper birch	*Betula*	*neoalaskana*
	0661	MAFU	Oregon crabapple	*Malus*	*fusca*
	0741	POBA2	balsam poplar	*Populus*	*balsamifera*
	0746	POTR5	quaking aspen	*Populus*	*tremuloides*
	0747	POBAT	black cottonwood	*Populus*	*balsamifera ssp. trichocarpa*

Table 3: FIA Alaskan Species Codes, Common names, and Latin names by Genus and Species.

7.5.3 Target Orbs

Professional orbs- https://shop.laserscanning-europe.com/Laser-Scanner-Reference-Sphere-Set-Basic_1 (Very expensive)

3D Orb models used in this study – Figure 15

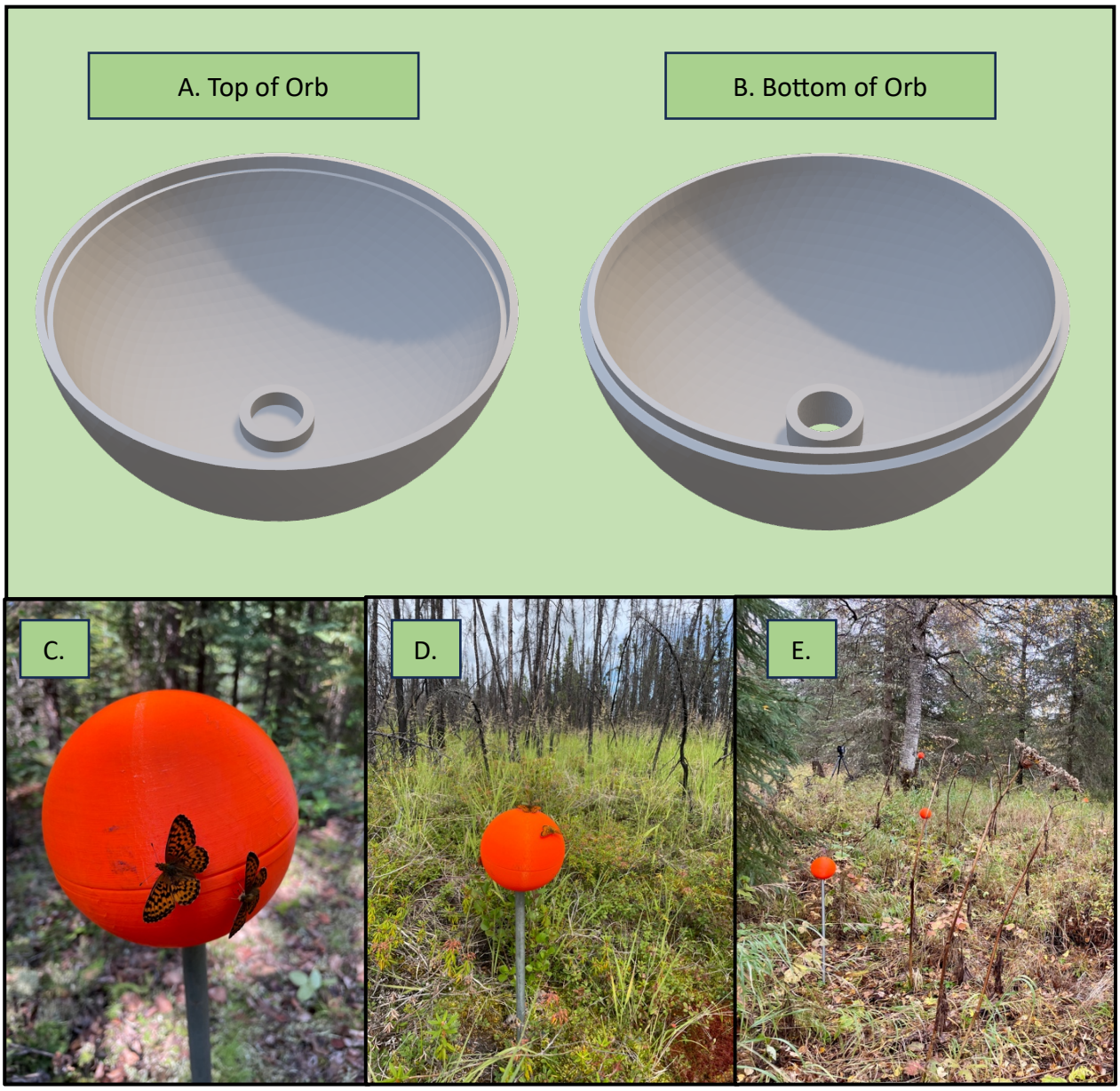

Figure 15: 3D model used to print target orbs. The orbs have a diameter of 145 mm. On the left, A is the top of the orb, it has an indentation on the inside rim and a circle in the center which the conduit fits into. On the right, B is the bottom of the orb, it has a matching indentation on the outside of the rim which locks with the top rim, and an open circle in the center which is used to mount the orb on the conduit. The 3D models were designed by Jonathan Batchelor (JonathanBatchelor.org). On the bottom, C, D, and E, show photos of the orbs being used in Alaska. Photos were taken by Rachel Deininger. Orange generally works well for target orb color because it is easy to find in a colored point cloud, making registering multiple scans and stitching them together easier.

7.5.4 Lidar

Objective of scan is to capture full subplot conditions ensuring scan proximity to small diameter veg to accurately measure DBH.

7.5.5 Terrestrial Laser Scanning (TLS)

7.5.5.1 Plot Setup

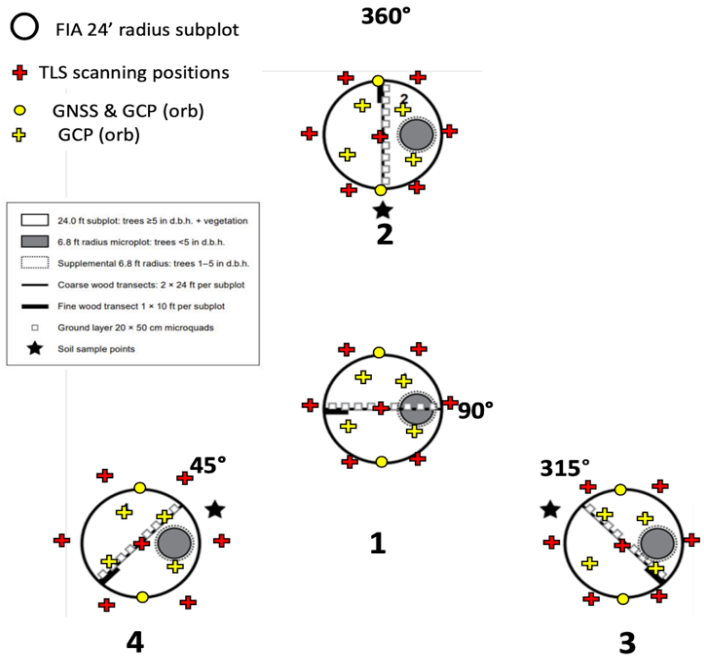

Figure 16: Terrestrial Laser Scanner Protocol. Scan positions are marked in red and Ground Control Points (GCP) are marked in yellow. Path diagrams are overlayed on FIA sampling protocol (soil sampling point, microplots and course woody material (CWM) line).

Find subplot center

- Setup tripod and scanner on subplot center
- Lock scanner to tripod with the knob on the base of the scanner

Setup orbs, Ground Control Points (GCP) Figure 16

- Sites will need 5 to 12 orbs depending on the density of the vegetation and visibility on one scan site to the next.
- Place an orb on both the farthest North and South points in the subplot. Orbs should be mounted on conduit, so they look like lollipops and are off the ground. This raises the orb out of any ground vegetation, longer conduits can be used in the shrubbery is too dense for scans.
- Orbs are depicted with yellow in Figure 16, the circles are north and south orbs while the checks are the rest.

Mark scanning positions

- Before initiating the first scan think about the subplot as a whole and decide how many scans will be needed to prevent any occlusion from occurring. Each scan individually will have occluded areas, but when put together you should be able to see each tree trunk from every side.

- Tag 3 to 6 scanning position outside the perimeter in addition to plot center. These scanning positions should be set back a step from the subplot perimeter, so they get a better angle looking in on the circle.
- From each scanning position, three orbs should be visible, and each orb needs to be seen by two scanners to be effective in processing. The more orbs visible by the scanner the easier the scans are to combine later. Branches, leaves and twigs may block orb visibility, what you can see is not always what the scanner can see.

7.5.5.2 Faro Focus

- Check scanner is locked to tripod
- Turn on scanner set parameters, Resolution: ¼, Quality: 4x
- Check that SD card and battery are inserted
- Adjust height of tripod until Faro is level
- Remove foam from lens and it ready to start scanning.

7.5.5.2.1 Scanning

- Check that scanner is locker to tripod, remove protective cover from lens, and check tilt of the scanner to make sure it is level.
- Begin scanning and remove yourself from line of sight.
- Name scans in a logical manner that is consistent and indicates where you are and the plot, subplot, and scan number.
- Sketch plot while scans are running (you will have time). This is helpful for finding orbs later in processing.

7.5.5.3 Leica BLK 360

*With the Leica we only collected a single scan from the center of the subplot.

- Set up tripod in center of subplot and check that it is level
- Mount scanner

7.5.5.3.1 Scanning

Turn on

- Press power button (begins flashing yellow)

Start Scanner

- Press power button (scanner will begin to flash yellow and audibly start to spin) Scanner must stay still
- Walk far enough away from scanner or behind obstacle so you don't appear in the scan

7.5.6 MLS

7.5.6.1 Comparison of SLAM Implementation in Leica BLK2GO and ZEB-HORIZON

7.5.6.1.1 Similarities in SLAM Implementation

Core Functionality:

- Both Leica BLK2GO and ZEB-HORIZON use SLAM (Simultaneous Localization and Mapping) algorithms to combine real-time position data with laser scan measurements, creating accurate 3D point clouds without reliance on external GNSS.

- Both devices rely on environmental features to maintain localization and mapping accuracy. Key to their SLAM operation is the ability to repeatedly scan identifiable features in the environment.

Integration of Sensors:

- Both systems use Inertial Measurement Units (IMU) in combination with LiDAR data for motion tracking and trajectory estimation, enhancing SLAM performance in environments where GNSS signals are unreliable.

Feature Dependency:

- Both devices require environments with sufficient static and identifiable features for optimal SLAM operation. They struggle in feature-poor environments like open fields or smooth corridors. Recommendations, such as augmenting environments with artificial features, are shared across both systems.

Loop Closure:

- Both devices utilize loop closure techniques to minimize cumulative drift errors. Returning to a previously scanned position allows the SLAM algorithm to reconcile trajectory errors.

7.5.6.1.2 Differences in SLAM Implementation

Primary Application and Form Factor:

- The Leica BLK2GO is designed for handheld operation with a focus on portability and ease of use in architectural, engineering, and construction applications. Its SLAM operation includes seamless recording as the user walks through an area.
- The ZEB-HORIZON is more versatile, supporting both handheld use and mounting on vehicles or platforms. It emphasizes mapping in challenging environments like forests or caves, where terrain variability can complicate trajectory estimation.

Feature Handling and Recommendations:

- The ZEB-HORIZON SLAM algorithm is more explicitly designed for challenging environments. It provides detailed guidance for scanning feature-poor spaces (e.g., adding artificial features or transitioning slowly through doorways). This suggests greater adaptability to complex scenarios.
- The BLK2GO focuses on maintaining high scanning quality in typical urban or interior environments and provides fewer adjustments for complex, feature-poor settings.

Scanning Capabilities:

- The ZEB-HORIZON has a longer effective range of up to 100 meters, ideal for larger-scale outdoor environments. The BLK2GO, in contrast, is optimized for shorter-range scanning in more confined settings

7.5.6.2 Plot Setup

Find subplot center

- Setup orbs, Ground Control Points (GCP)
- Set up a north and a center orb. For smaller scans only the north and center orb are necessary. If you are piecing together multiple larger scans, more orbs should be set up in appropriate locations, see TLS protocol for reference.
- Reference above section for similarities

Triangle (Figure 17 A.)

- For the triangle path, the user starts at subplot center and walk in numeric order in triangular formation around the subplot.
- The user will follow the green line in Figure 5a. Starting by going north till they have passed outside the subplot, turning and walking directly southeast for approximately 58 ft before turning west and returning to plot center. Then triangle two is walked.

Lawnmower (Figure 17 B.)

- For the lawnmower path, the user starts at subplot center and walks a horizontal, vertical, or diagonal transect of the subplot depending on which of the four it is.
- For the one in Figure 5b, it is vertical along the green line. They user will end at the east side and make their way to the south east corner where they will begin their grid pattern walk across the subplot.
- From the bottom left corner, they will walk straight north turn east, walk approximately 12.5 ft and turn to walk back south. This is continued until the whole subplot is scanned.

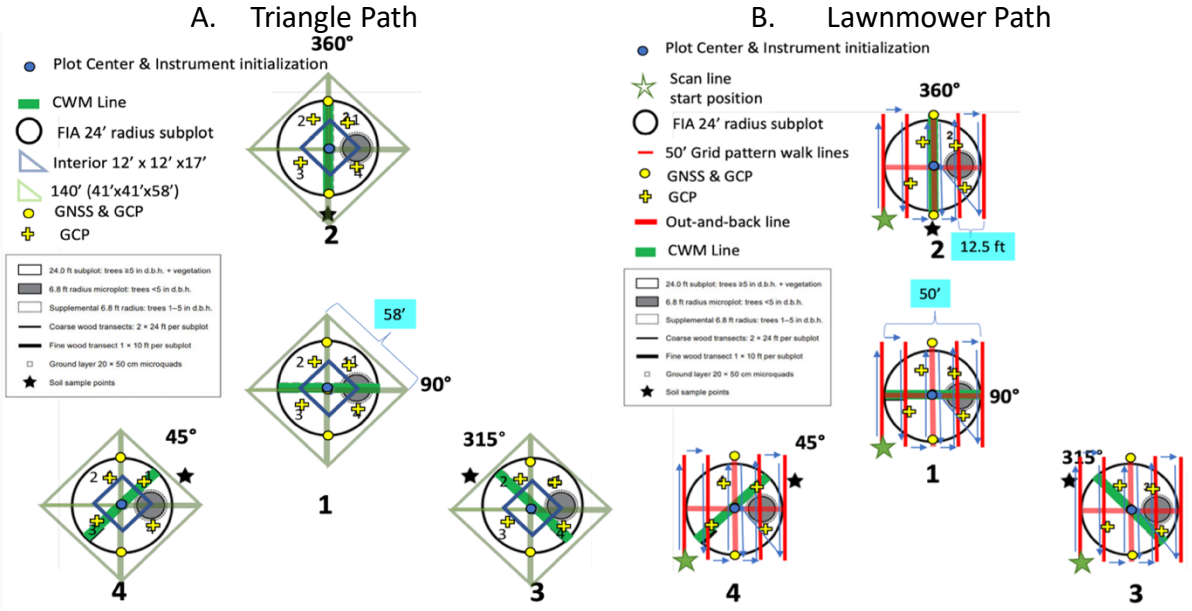

Figure 17: Mobile Laser Scanning Protocol: The Triangle path (A.) on the left and the Lawnmower path (B.) on the right. Path diagrams are overlayed on FIA sampling protocol (soil sampling point, microplots and course woody material (CWM) line).

7.5.6.3 Zeb Horizon

7.5.6.3.1 Scanner setup

- Attach battery to Datalogger
- Turn Datalogger by pressing the power button
  - Will light up green when on (Figure 18)
- Attack cable from Datalogger to scanner
  - When ready for scan to start it will have a walking red light (Figure 18)
- Start Scan Scanner

- Start with device facing north, unless north has an obstruction within 6 feet of scanner. Scanner must be held perfectly still during the startup and initializing process.
- Hold button down on scanner until you hear a beep, the light will change solid red. The light will begin flashing yellow to indicate it is initializing. Once the light is solid green, the scan begins.
- Record scans start time, this will be important for identifying files when downloading data.

	Data Logger LED		Scan head LED array
	REVO	DATA	
Data logger booting up.	✱	-	-
Connecting to scan head.	●	-	●●●●
Standby mode	●●	-	●○○○
Initiate new scan Long press the function button on either the scan head or the data logger until the REVO LED and scan LED array light solid red to initiate a new scan	●	-	●●●●
Initialization mode The scan head must remain stationary for a period of 15 seconds. If the scan head is disturbed during initialisation the system will revert to standby mode (Step 4)	✱	-	✱✱✱✱
Scanning mode After the 15 second initialization, the REVO LED and scan head LED array will light green and the scan head will start rotating. Pick up the scanner and conduct the scan.	●	-	●●●●
End scan - Data formatting To end the scan, long press the function button on either the scanner head or the data logger until the scan head stops rotating. The DATA LED will light orange while the scan data is converted to the required output format	●●	●	●○○○

Figure 18: Zeb LED lights during scanner startup and scanning(1)

7.5.6.3.2 Scanner Setup

- Follow prescribed protocol unless experiencing SLAM errors
  - Begin by walking in a small circle so the scanner can orient itself.
  - Walk one of the paths described above, Lawnmower or Triangle.
  - Hold position for 10 seconds to take a georeferenced point.

7.5.6.4 BLK2GO

7.5.6.4.1 Scanning

- Turn on
  - Press power button (begins flashing yellow)

    - Set on Stand (Once device turns green it is ready to begin scanning)
- Pair Scanner with Phone (BLK2GO Live app) – QR code under battery
    - By default, image compression is on.
    - Allows you to see a less detailed version of the scan in real time with the path you are taking.

7.5.6.4.2 Scanning

- Start Scanner
    - press power button (scanner will begin to flash yellow and audibly start to spin) Scanner must stay still.
    - Once light turns green and points begin to show on phone you and begin walking around.
- How to Hold Scanner While Scanning
    - Hold directly out in front of you because it will filter out a slice directly behind it, so you are not caught in the data.
    - The speed you walk will directly affect your data. Walking slower will collect a more detailed scan.
    - A quick press of power button will collect a photo.
- Stop Scan – return to stand, press and hold power button for 3 seconds.

7.5.6.5 Trouble Shooting SLAM errors

- Error due to slope
    - Begin scan at corner near the lowest point in plot area and work your way up hill following the spirit of the lawnmower pattern were the long transects are perpendicular to the dominant slope direction.
    - Keep scanner level to the ground. If going downhill and pointing downhill, inclined the scanner downhill to match the slope. If side hilling perpendicular to the slope, tilt the scanner to match the slope and similarly when walking up hill, incline the scanner up.
    - The steeper the slope, the more important this step is. Follow the green-yellow-red queues provided by the real-time output from BLK2GO to determine if more or less inclination of the scanner is required.
- Dense conditions that create narrow corridors
    - Follow the spirit of the protocol as best as possible. Avoid going THROUGH dense areas or narrow corridors, instead pointing the scanner into the dense areas and circumnavigating the dense patch to capture conditions in the patch without entering it.
    - When passing through narrow corridors, do not walk the scanner through in front of you, instead follow the Leica protocol for going through doorways. Summarized as orienting sideways and going slow. If very narrow orient the scanner behind you and walk through the narrow and maintain that orientation while moving the scanner left and right until you enter an opening where you can re orient the scanner in front of you in the direction of movement.

7.5.7 ALS

7.5.7.1 G-LiHT

ALS scans were collected using NASA Goddard's Lidar, Hyperspectral, and Thermal (G-LiHT) airborne imaging system (Cook et al., 2013), which has been flown extensively over Southern and Interior Alaska, including the Campbell Tract Special Recreation Management Area (CTSRMA) and Bonanza Creek Experimental Forest (BCEF) during the summer of 2022. The G-LiHT system, equipped with a Riegl VQ-480 Airborne Laser Scanner, flew at an altitude of 335 meters above ground level (AGL), collecting data at a pulse repetition rate of up to 300 kHz, yielding 150,000 points per second. Point spacing was 0.23 meters along flight lines and 0.57 meters between lines, providing a detailed point cloud with a 10 cm laser footprint, ideal for detecting fine-scale vegetation structure. The vertical accuracy was maintained at 10 cm, with GPS and Inertial Navigation System (INS) ensuring precise georeferencing.

7.5.8 Imaging Protocol

Use the Survey123 companion app to take photos of the four predetermined locations found 12 ft away from subplot center in the cardinal direction North, South, East, West. Take images every 45 degrees (8 images total) starting at magnetic north and moving clock- wise.

7.5.9 Downloading Data

7.5.9.1 Zeb Horizon

7.5.9.1.1 Extracting Data

- Attach battery pack to data logger and turn on data logger.
- Wait a few minutes for it to bootup and lights to quit flashing plug-in thumb drive. Green data light should come on when green data light turns off data is loaded onto thumb drive plug thumb drive into computer copy all files with .geoslam extension into folder on your computer.
    - Rename files with location_year_month_day_plot_subplot_scan attempt.geoslam
    - Ex: Fairbanks_2023_07_01_80084_1_scan_xx.geoslam

7.5.9.1.2 Zeb Connections

- All point cloud files created by Zeb are in the .geoslam format.
- To convert into Laz files, they must be imported into either Zeb Hub or Zeb Connections. For this project we used GeoSLAM Connections.

7.5.9.1.3 GeoSLAM Connections:

- Create and name a project folder
- Drag and drop files into import folder
- Select .las for-export format, 10 mm for spatial decimation of point cloud, Forest for SLAM Processing Type, and click the check boxes for Remove outlies from data and remove moving objects from data. These will both increase Processing time. Once the settings are all set, press import.
- This will create several files of which we will use the Laz file and the trajectory file.

7.5.9.2 BLK2GO

7.5.9.2.1 Connect to Scanner:

Connect your computer to the BLK2GO scanner via Wi-Fi or USB cable.
For Wi-Fi, use the SSID and password listed inside the scanner's battery compartment.

7.5.9.2.2 Open Cyclone REGISTER 360:

- Launch the Cyclone REGISTER 360 software.
- Create a new project or open an existing one.

7.5.9.2.3 Import BLK2GO Data:

- Click the BLK2GO button to open the connection dialog.
- Select the scanner from the available list. If not visible, click Re-Scan.
- After connection, click Add to Project to display the list of available "Walks."
- Check the boxes for the desired Walks to import and click Import.

7.5.9.2.4 Export to E57:

- In the import panel, check the box for Export E57 to folder (located in the lower-right corner).
- Choose a folder on your computer to save the E57 files.
- Click Import to begin the process. Cyclone will create the E57 files directly without importing the data into the project.

- Save the Files:
  - Ensure the E57 files are saved to the designated folder.
  - Back up the raw BLK2GO files for redundancy if needed.

7.5.9.3 Faro Focus

- Data is stored on the SD card, remove this from scanner and connect to your device to download data.
- Faro files are .fls

7.5.9.3.1 Registration in Faro Scene

Processing settings:

- Filter = stray point and distance filters
- Find spheres – 0.145
- Preform automatic registration (target based)
- Find correspondences for scan positions
- TDT: 0.001

7.5.9.3.2 Cloudcompare

- Clean up floating points
- Subsample PC 0.01 m level

7.5.9.4 Leica 360

7.5.9.4.1 Power On the Device:

- Press and hold the power button. The ring-shaped LED will blink yellow, indicating startup, and turn solid green when the device is ready.

Establish Connection to a Computing Device:

- Connect the BLK360 to a computer either wirelessly (Wi-Fi) or via a USB-C Gigabit-Ethernet adapter.
- For Wi-Fi:
  - Select the BLK360 network in your computer's Wi-Fi settings (SSID is "BLK360-XXXXX").
  - Enter the password, found on the label in the battery compartment.
- For Ethernet:

- Use a USB-C Gigabit-Ethernet adapter to connect the device to the computer or LAN infrastructure.

Launch Leica BLK Data Manager:

- Use the Leica BLK Data Manager software to detect and connect to the BLK360.
- Ensure the device and computer are in the same subnet if using a LAN connection.

7.5.9.4.2 Downloading Data

Initiate Data Transfer:

- Once connected, the BLK Data Manager software will display available scans stored on the device.
- Select the desired scans for transfer.

Transfer Scans:

- Scans are downloaded to the computer as raw data.
- The transfer process includes metadata and point cloud information.

Processing and Saving as .fls Files

7.5.9.4.3 Save Data in .fls Format:

- After transferring the scans to the computer, the BLK Data Manager software can convert them to .fls files.

7.6 On grid-FIA plots

Field tecs are required to sign a non-disclosure agreement before learning the locations of all on grid FIA plots. On grid-FIA plot locations are kept a secret to prevent any intentional tampering that could affect the site's integrity. These locations will not be revealed to the public at any point.

7.7 Work Cited

https://geoslam.com/wp-content/uploads/2021/02/ZEB-Horizon-User-Manual-v1.3.pdf (zeb manual)

https://www.fs.usda.gov/research/sites/default/files/2023-04/pnw-2023_alaska_fia_field_manual.pdf (FIA manual)

https://forestry.org/wp-content/uploads/2021/10/1-26-21-Presentation-SAF.pdf (PowerPoint Miho)

Andrew T Hudak, Patrick A Fekety, Van R Kane, Robert E Kennedy, Steven K Filippelli, Michael J Falkowski, Wade T Tinkham, Alistair M S Smith, Nicholas L Crookston, Grant M Domke, Mark V Corrao, Benjamin C Bright, Derek J Churchill, Peter J Gould, Robert J McGaughey, Jonathan T Kane, and Jinwei Dong, “A carbon monitoring system for mapping regional, annual aboveground biomass across the northwestern USA” Environmental Research Letters, September 2020, vol. 15

Anthony G. Vorster, Paul H. Evangelista, Atticus E. L. Stovall, and Seth Ex, “Variability and uncertainty in forest biomass estimates from the tree to landscape scale: the role of allometric equations” Carbon Balance Management, December 2020, vol. 15

Can Vatandaşlar and Zeybek Mustafa, “Application of handheld laser scanning technology for forest inventory purposes in the NE Turkey” TURKISH JOURNAL OF AGRICULTURE AND FORESTRY, June 2020, vol. 44

Cook, B. D., L. W. Corp, R. F. Nelson, E. M. Middleton, D. C. Morton, J. T. McCorkel, J. G. Masek, K. J. Ranson, V. Ly, and P. M. Montesano, “NASA Goddard's Lidar, Hyperspectral and Thermal (G-LiHT) airborne imager” Remote Sensing, 2013

Daniel Kükenbrink, Mauro Marty, Ruedi Bösch, Christian Ginzler, “Benchmarking laser scanning and terrestrial photogrammetry to extract forest inventory parameters in a complex temperate forest” International Journal of Applied Earth Observation and Geoinformation, August 2022, vol. 113

Dengsheng Lu, “The potential and challenge of remote sensing-based biomass estimation” International Journal of Remote Sensing, November 2005, vol. 27

Elizabeth A. LaRue, Franklin W. Wagner, Songlin Fei, Jeff W. Atkins, Robert T. Fahey, Christopher M. Gough, and Brady S. Hardiman, “Compatibility of Aerial and Terrestrial Lidar for Quantifying Forest Structural Diversity” Remote Sensing, April 2020, vol. 12

Guancheng Liu, Guoyong Yan, Mengyu Chang, Binbin Huang, Xingyu Sun, Shijie Han, Yajuan Xing, Qinggui Wang, “Long-term nitrogen addition further increased carbon sequestration in a boreal forest” European Journal of Forest Research, October 2021

Hank A. Margolis, Ross F. Nelson, Paul M. Montesano, André Beaudoin, Guoqing Sun, Hans-Erik Andersen, and Michael A. Wulder, “Combining satellite Lidar, airborne Lidar, and ground plots to estimate the amount and distribution of aboveground biomass in the boreal forest of North America” NRC Research Press, July 2015, vol. 45

Hong Chi, Guoqing Sun, Jinliang Huang, Zhifeng Guo, Wenjian Ni, and Anmin Fu, “National Forest Aboveground Biomass Mapping from ICESat/GLAS Data and MODIS Imagery in China” Remote Sensing, May 2015, vol. 7

Hyungwoo Lim, Ram Oren, Torgny Näsholm, Monika Strömgren, Tomas Lundmark, Harald Grip1 and Sune Linder, “Boreal Forest biomass accumulation is not increased by two decades of soil warming” Nature Clime Change, January 2019, vol. 9

Juha Hyyppä, Anttoni Jaakkola, Yuwei Chen, Antero Kukko, Harri Kaartinen, Lingli Zhu, Petteri Alho, Hannu Hyyppä, “Unconventional LIDAR Mapping from Air, Terrestrial and Mobile.” Photogrammetric Week, 2013

Lena Schulte-Uebbing and Wim de Vries, “Global-scale impacts of nitrogen deposition on tree carbon sequestration in tropical, temperate, and boreal forests: A meta-analysis” Global Change Biology, February 2018, vol. 24

Marius G. Heidenreich and Dominik Seidel, “Assessing Forest Vitality and Forest Structure Using 3D Data: A Case Study From the Hainich National Park, Germany” Frontiers in Forests and Global Change, June 24, 2022, vol. 5

P.M. Montesano, R.F. Nelson, R.O. Dubayah, G. Sun, B.D. Cook, K.J.R. Ranson, E. Næsset, V. Kharuk, “The uncertainty of biomass estimates from Lidar and SAR across a boreal forest structure gradient” Remote Sensing of Environment, April 2014, vol. 154

Sébastien Bauwens, Harm Bartholomeus, Kim Calders, and Philippe Lejeune “Forest Inventory with Terrestrial Lidar: A Comparison of Static and Hand-Held Mobile Laser Scanning” Forests, June 2016, vol. 7

Steven Wagers, Guillermo Castilla, Michelle Filiatrault, and G. Arturo Sanchez-Azofeifa, “Using TLS-Measured Tree Attributes to Estimate Aboveground Biomass in Small Black Spruce Trees” Forests, November 2021, vol. 12

Ville Kankare, Markus Holopainen, Mikko Vastaranta, Eetu Puttonen, Xiaowei Yu, Juha Hyyppä, Matti Vaaja, Hannu Hyyppä, Petteri Alho, “Individual tree biomass estimation using terrestrial laser scanning” ISPRS Journal of Photogrammetry and Remote Sensing, January 2013, vol. 75

Yi Lin, Anttoni Jaakkola, Juha Hyyppä and Harri Kaartinen, “From TLS to VLS: Biomass Estimation at Individual Tree Level” Remote Sensing, July 2010, vol. 2

Yifan Qiao, Guang Zheng, Zihan Du, Xiao Ma, Jiarui Li, and L. Monika Moskal, “Tree-Species Classification and Individual-Tree-Biomass Model Construction Based on Hyperspectral and Lidar Data” Remote Sensing, February 2023, vol. 15

“Study Sites & Design: Bonanza Creek Experimental Forest,” “Study Sites & Design: Caribou-Poker Creeks Research Watershed,” Institute of Artic Biology, University of Fairbanks Alaska (UFA), https://www.lter.uaf.edu/research/study-sites-bcef, https://ww.lter.uaf.edu/research/study-sites-cpcrw

“Campbell Tract Special Recreation Management Area” US Department of Interior, Bureau of Land Management (BLM), https://www.blm.gov/visit/campbell-tract

8 Appendix B. Metadata doc

8.1 Objectives

This field work will help the development of sampling techniques using terrestrial Lidar scanners, applying a combination of terrestrial and airborne Lidar and manual sampling methods. The field work took place in Alaskan boreal forests outside of Anchorage in the summer of 2022. The objective is to accurately determine forest biometrics such as aboveground biomass with fine scale terrestrial scanning and scale it up to airborne scanning to increase the accuracy and potential of large-scale airborne scans in boreal forests.

The Forest inventory Analysis (FIA) program in Alaska and more broadly the US Forest Service will benefit from this project. The sampling sites will be on preexisting FIA plots, which are manually sampled on a ten-year basis. Not only will this study be beneficial for the parties involved but for a range of scientists seeking to better understand how Lidar technologies can be used to assess and measure forest variables. This work will help push the boundaries of what Lidar technology can be used for providing insight into the shortcomings and strengths of terrestrial Lidar technology. Companies developing Lidar technology will be able to learn from the performance of different scanners in the novel boreal forest environment. The first stage of this project will compare multiple scanners in their usability in the field and how they handle dense vegetation.

8.2 Background

8.2.1 Study Areas.

8.2.1.1 Anchorage- Campbell Tract Special Recreation Management Area

The initial sampling strategy was tested in Campbell Tract Special Recreation Management Area (CTSRMA) adjoined to Far North Bicentennial Park in Anchorage Alaska over a period of two weeks between September 12th, 2022, and September 23rd, 2022. Campbell Tract is a Beurre of Land Management owned recreation area with 730 acres of forest (BLM). This location was chosen for its easy accessibility and proximity to Anchorage, similar forests

characteristics to interior Alaska, and field measurements taken manually by FIA crews are available for the established plots.

8.2.1.2 Fairbanks- Bonanza Creek Experimental Forest and Caribou-Poker Creek Research Watershed

The second phase of sampling was in Bonanza Creek Experimental Forest (BCEF) outside of Fairbank Alaska for six-weeks between June and August 2023. These sites were chosen for their accessibility from the city of Fairbanks, the presence of pre-established FIA plots, and the ecological gradient across the parks is archetypal of interior Alaska's boreal forests (University of Fairbanks Alaska). Throughout the Yukon River watershed and around Fairbanks the ecoregions are classified as Interior Alaskan-Yukon Lowland Taiga and Yukon Interion Dry Forest (Margolis et al. 2015). At BCEF, there are statistically sufficient field plots and Airborne scans to represent interior Alaska's boreal forests allowing us to apply small sized sampling to a regional scale.

8.2.2 FIA

Lead by US Forest Service, Forest Inventory Analysis (FIA) program is a nationwide inventory of all forested lands (>10% forest coverage). Data from FIA is used to estimate forest area by forest type and stand size, tree statistics by species and size, the health of the forest, and monitor change over time. Alaskan FIA varies from the lower 48 by having a lower sample intensity with one plot every 30,000 acres. Interior Alaska FIA also utilizes remote sensing in the form of Lidar, hyperspectral, thermal, and fine scale RGB.

8.2.2.1 Plot Arrangement

Plots are a circle broken up into four subplots. Subplots are 48 ft diameter circles spaced evenly apart with one at plot center, two is directly north, three is to the southeast, and four is to the southwest (Appendix A. Figure 13). The subplot center of each subplot is 120 ft away from the plot center.

Sub plots are outfitted with pins to visually mark locations making them easier for field technicians to find and survey. The pins are plastic, about two feet long, and come in three different colors white, yellow, and red. For each subplot there is a single white pin at the center, two yellow pins 12 ft east and west from the center, and four red pins radiating out in the woody transect lines which vary from subplots 1 through 4. For the purpose of this study the pins were only used for locating the subplots centers.

8.2.2.2 Witness Trees

Witness trees are chosen for each subplot so the center can be relocated if the pins get removed or destroyed in the 10 years between visits. They are tagged with yellow circles or silver diamonds made of metal and nailed to the tree oriented towards subplot center. The distance between subplot center and azimuth are recorded and stored for future use.

8.3 Data

8.3.1 Device Features

Table 4: Comparing Lidar Metrics for TLS and MLS Devices

Type	*Device*	*Measurement speed (points/sec)*	*Range (m)*	*Wavelength (nm)*	*Price (USD)*

TLS	*Leica BLK 360*	*680,000*	0.5 – 45 m	830	$25,900
	Faro Focus S350	976,000	0.6-350 m	1550	$25,500
MLS	*Leica BLK2GO*	*420,000*	0.5 – 25 m	830	$52,995
	ZEB Horizon	300,000	100 m	903	$57,600

8.3.2 Scans per device for Anchorage and Fairbanks

Table 5: Plots Scanned by Device, Anchorage and Fairbanks Field Seasons.

Anchorage 2022				
Type	*Device*	Total Plots	Total Subplots	Total Scans
TLS	*Leica BLK 360*	7	26	26
	Faro Focus S350	7	20	113
MLS	*Leica BLK2GO*	7	36	36
	ZEB Horizon	7	37	37
ALS	*G-LiHT*	7	27	1
Fairbanks 2023				
MLS	*ZEB Horizon*	43	165	165
ALS	*G-LiHT*	43	172	1

8.4 Data Matrices

8.4.1 Anchorage Matched Trees FIA with FARO Metadata Attributes Table

Table 6: MatchesFIAFARO.csv

Column Head	type	Metrics	Notes
Plot	int	NA	FIA Plot identification number
subplot	int	NA	Subplot 1 – 4 for each plot (not all subplots were scanned with each device)
dens_threshhold	num	0-1	Density threshold, a parameter set when running Spanner
eigen_threshold	num	0-1	Eigen value threshold, a parameter set when running Spanner
FIA_ID	chr	NA	A number that represents each unique plot, subplot, density threshold, eigen threshold, FIA, and unique tree ID combination. Since FIA is not run through Spanner there is not density threshold or eigen threshold, they are filled in by

			NA to keep the ID length the same for FARO_ID and FIA_ID Ex: 100.1.NA.NA.FIA.147
FIAID	int	NA	Unique tree ID
FIA_x	num	meters	X coordinate location of FIA recorded tree in local coordinate system
FIA_y	num	meters	Y coordinate location of FIA recorded tree in local coordinate system
FIA_DBH	num	centimeters	DBH measured manually by FIA crew
FIA_Height	num	meters	Height measured manually by FIA crew
FARO_ID	num	NA	A number that represents each unique plot, subplot, density threshold, eigen threshold, FARO, and unique tree ID combination. Ex: 100.1.0.4.0.5.FARO.147
FAROID	int	NA	Unique number given to each TLS measured tree
FARO_x	chr	meters	X coordinate location of FARO tree found using Spanner package, in local coordinate system
FARO_y	num	meters	Y coordinate location of FARO tree found using Spanner package, in local coordinate system
FARO_DBH	num	centimeters	DBH calculated from segmented point cloud using Spanner
FARO_Height	num	meters	Height of individual tree point cloud, calculated using ITSME package
Species	int	94, 95, 375, 747	Tree Species recorded by FIA in the field using FIA Codes (Appendix A Table 4).
DBHDiff	num	centimeters	Absolute value of FARO_DBH minus FIA_DBH
HeightDiff	num	meters	Absolute value of FARO_Height minus FIA_Height
Proximity	Int		Number of trees within a meter of the given tree
Volume	num	m^3	Alpha volume of individual tree point cloud calculated using ITSME package
ProjectedArea	num	M^2	Projected crown area of individual tree point cloud calculated using ITSME package
Distance	num	meters	Distance between matched tree, calculated with between (FIA_x, FIA_y) and (FARO_x, FARO_y)
Biomass_FARO	num	Kg/m^3	Biomass estimate calculated using species specific allometric equation, DBH, and Height from FIA recorded data
Biomass_FIA	num	Kg/m^3	Biomass estimate calculated using specific allometric equation, DBH, and Height from TLS calculated metrics
unqtest	chr	N/A	Combined density threshold and eigen threshold values to make a unique test code. Ex: 0.4.0.5

unqPS	num	N/A	A number that represents each unique plot and subplot combination. Ex: 100.2 is plot 100 subplot 2
Biomass_Diff	num	Kg/m^3	Absolute value of Biomass_FARO minus Biomass_FIA
Match	logi	True or False	True matches between FIA and TLS measures trees are withing 2 meters of each other and have less than 5 meter height difference

8.4.2 Anchorage TLS Metadata Attributes Table

Table 7: FARODataAll.csv

Column Head	type	Metrics	Notes
unq	chr	NA	
Plot	int	NA	FIA Plot identification number
subplot	int	NA	Subplot 1 – 4 for each plot (not all subplots were scanned with each device)
dens_threshhold	num	0-1	Density threshold, a parameter set when running Spanner
eigen_threshold	num	0-1	Eigen value threshold, a parameter set when running Spanner
ForestType	chr	NA	Which forest type, deciduous, black spruce, or mixed the plot is in
Device	chr	NA	Which method of data collection used; in this case they are all FARO
CenterX	num	meters	X coordinate for plot center
CenterY	num	meters	Y coordinate for plot center
TreeID	int	NA	Unique number assigned to each tree
FARO_DBH	num	centimeters	DBH calculated from segmented point cloud using Spanner
FARO_Height	num	meters	Height of individual tree point cloud, calculated using ITSME package
Volume	num	m^3	Alpha volume of individual tree point cloud calculated using ITSME package
ProjectedArea	num	M^2	Projected crown area of individual tree point cloud calculated using ITSME package
Error	num	percent	Error measurement created when running Spanner
Distance	num	meters	Distance between matched tree, calculated with between (FIA_x, FIA_y) and (FARO_x, FARO_y)

unqPS	num	N/A	A number that represents each unique plot and subplot combination. Ex: 100.2 is plot 100 subplot 2
n	int	count	Number of trees on plot
density_INDIV_all	num	count	Number of trees within a meter of measured tree
ratio	num	ratio	Ratio between DBH and Height
ratio_within_original_bounds	logi	True or False	Is the ratio measurement withing the same range of ratios created by the FIA trees
ratio_within_adjusted_bounds	logi	True or False	Is the ratio measurement withing the same range of ratios created by the FIA trees with a 15% adjustment of the range
PAHeight	num	ratio	Projected Area divided by height
VolumeHeightt	num	ratio	Volume divided by height
Predicted_Species	Factor	94, 95, 375, 747	Tree species predicted with random forest model
Biomass_FARO_estt	num	Kg/m^3	Estimate biomass for each tree

8.4.3 Anchorage FIA Metadata Attributes Table

Table 8: FIADataAll.csv

Column Head	type	Metrics	Notes
unq	chr	NA	A number that represents each unique plot, subplot, density threshold, eigen threshold, FIA, and unique tree ID combination. Since FIA is not run through Spanner there is not density threshold or eigen threshold, they are filled in by NA to keep the ID length the same for FARO_ID and FIA_ID Ex: 100.1.NA.NA.FIA.147
Plot	int	NA	FIA Plot identification number
subplot	int	NA	Subplot 1 – 4 for each plot (not all subplots were scanned with each device)
dens_threshhold	num	0-1	For FIA this is always NA
eigen_threshold	num	0-1	For FIA this is always NA
Device	chr	NA	Which method of data collection used; in this case they are all FIA
CenterX	num	meters	X coordinate for plot center

CenterY	num	meters	Y coordinate for plot center
TreeID	int	NA	Unique number assigned to each tree
Species	int	94, 95, 375, 747	Tree Species recorded by FIA in the field using FIA Codes (Appendix A Table 4).
Status	int	1 or 2	1 means the tree is living, 2 means the tree is dead
DBH	num	centimeters	DBH measured manually by FIA crew
Height	num	meters	Height measured manually by FIA crew
DistancetoCenter	num	meters	Distance between center of plot and tree location measured by FIA crew
Loc_X	num	meters	X coordinate location of FIA recorded tree in local coordinate system
Loc_Y	num	meters	Y coordinate location of FIA recorded tree in local coordinate system
unqPS	num	N/A	A number that represents each unique plot and subplot combination. Ex: 100.2 is plot 100 subplot 2
n	int	count	Number of trees on plot
ratio	num	ratio	Ratio between DBH and Height
Biomass_FIA	num	Kg/m^3	Estimate biomass for each tree

9 Appendix C. Proposal

The following proposal was submitted for the Gloria Baron Wilderness Society Scholarship in April 2024 and awarded funding in August 2024.

9.1 Wilderness Monitoring Proposal

Climate change will remake the Alaskan wilderness. Land managers and stewards must decide where to resist these changes, accept them, or help direct them to new ecosystem states. This study will provide crucial knowledge to assist in tracking ecological trajectories.

Boreal forests as we know them are disappearing and are in danger of vanishing over the next century. Boreal forests are universally at risk of type conversion due to climate change. No laws or regulations can prevent the current effects of climate change on wilderness areas. Wilderness areas in Alaska are particularly, due to their large extent, difficult to access, and many do not allow permanent monumentation. We must develop methods for monitoring these landscapes to better predict how they are changing and to create informed solutions to mitigate negative consequences while preserving the imperiled ecosystems for all communities that depend on them, wild and human.

How do we identify where type conversion is occurring across large wilderness areas? **My research goal is to develop methods for monitoring forest state changes in wilderness landscapes experiencing climate impacts.** I propose to use state-of-the-art resources to develop

a long-term forest structure monitoring protocol that will allow us to identify areas of type conversation and inform future-oriented conservation and management.

I developed this proposal after leading two field campaigns in the threatened Alaskan wilderness to collect the data that would be used in this project. I collaborated with the US Forest Service and Alaska Division of Natural Resources to implement novel data collection methods in the field. With the support of the Gloria Barron Wilderness Society Scholarship, I will be able to use my experience to develop innovative monitoring solutions to protect wilderness in Alaska.

9.1.1 Background

Alaska is the epitome of American wilderness, as defined in the 1964 Wilderness Act "an area where the earth and its community of life are untrammeled by man." In Alaska, wilderness is the landscape that surrounds pockets of human activity. Across this landscape, 70% are boreal forests. Although boreal forests are resilient and adapted to harsh conditions13,26,29, modern climate change far outpaces variability historically experienced by boreal forests.

With the Wilderness Society funding, I will provide managers with tools for monitoring remote wilderness areas across Alaska. This research tackles three objectives: **1)** Develop methods specific to Alaskan species to identify forest type conversion and forest resilience on a local and regional scale. **2)** Create a forest state monitoring plan to provide real-time knowledge about the state of landscape and state of change. **3)** Provide tools to assess Alaskan wilderness that cannot be assessed by fieldwork alone.

Ecological resilience is the ability of a system to maintain functions, structures, and feedback in response to disturbances[1]. A resilient system maintains a stable state, if the resilience of a system is exceeded it can transform into a new state with different properties[20]. For example, lowland boreal forests formerly occupied by black spruce are converting to sphagnum bogs, while spruce-dominated hillsides are transforming into deciduous forests[1]. On slopes with slow-draining soils, white spruce has been declining due to water stress caused by warming[24,25]. In lowland areas, drunken (i.e., partially or fully submerged[11]) forests are expanding as the permafrost thaws, resulting in black spruce leaning and falling[10]. If trends continue along the current IPCC-predicted trajectory, forest-type conversion is unavoidable[5, 6].

The boreal forests are changing, and managers need a decision-making process such as Resist-Accept- Direct (RAD) which is composed of three strategies to employ in response to ecosystem change[16]. Monitoring is an integral part of RAD as it guides land managers in selecting which strategy or mix of strategies is best and determining when and how to switch strategies as change continues. To doggedly resist ecosystem changes will prove futile, employing long-term monitoring is necessary for deciding what changes should be accepted and directing them towards the most sustainable option[16].

Remote sensing is any data acquired through observation of an object or phenomenon without making contact. This can be passively collected, for example, optical imagery, or actively collected, for example, radar or Lidar. Remote sensing devices can collect information on at different extents, from ground level to airborne, or spaceborne. Remote sensing addresses the challenges of monitoring wilderness areas with the ability to access and cover a large extent without establishing permanent monumentation. In remote sensing, Lidar (Light Detection and Ranging), is an active remote sensing method that creates a 3-dimensional image of the target object or area by measuring distance with lasers[3,15].

In this study, we mitigate the limitations of Lidar data by combining two sources: aerial laser scanning (ALS) and mobile laser scanning (MLS)[3,15]. By using data collected at nested levels of extent; local and regional scale, we can benefit from the accuracy of higher resolution ground data while upscaling measurements over a larger area2. Lidar is the most accurate remote sensing method for measuring forest structure and understanding how disturbances drive changes in forest structure [12,14,28]. Forest structural complexity is related to carbon storage, productivity, age, microclimate, and overall resilience [7-8, 19,22-23]. Therefore, by quantifying forest structural complexity, we can monitor overall forest function.

9.1.2 Study Area and Available Data

This study will use data from Bonanza Creek Experimental Forest (BCEF), a 5,053-ha wilderness research area near Fairbanks, Alaska, managed by the State of Alaska Division of Forestry30. This site was chosen for its accessibility from Fairbanks, the presence of pre-established Forest Inventory Analysis (FIA) plots, and the ecological gradient across the forest is archetypal of interior Alaska's boreal forests30. At the BCEF, there are statistically sufficient field plots and airborne scans to represent interior Alaska's boreal forests, allowing us to apply small-area sampling to a regional scale.

FIA and ALS data for this project has already been obtained from the US Forest Service and NASA. FIA surveys were conducted in BCEF during the summers of 2011, 2012, and 2023. ALS scans were collected with NASA Goddard's Lidar Hyperspectral and Thermal (G-LiHT) airborne remote sensing system[9] which has been flown over most of Southern and Interior Alaska, including the BCEF in the summer of 2014 and 2022. My team and I conducted MLS sampling in BCEF for six weeks in 2023. We collected a total of 165 scans using the Zeb Horizon, a handheld MLS device.

Many long-term studies on boreal forests have been conducted in BCEF. Chapin et al. (2010) made predictions for the permafrost, successional trajectories, and disturbance events in BCEF based on decades of research done there. They concluded that permafrost was most at risk in high ice-content lowlands and in areas with severe burning but would otherwise remain resilient to warming. Permafrost degradation can shift the ecosystem from black spruce forests to sphagnum bogs, herbaceous fens, or deciduous forests. Increasingly frequent disturbances, such as severe wildfires, will add to the landscape transformation. This project has the potential to build on previous work in BCEF and contributes to a collective body of knowledge studying arctic processes and ecosystems.

9.1.3 Methodology and Analysis

The aerial and mobile Lidar point clouds are clipped to the exact size of the FIA plots, so results are geospatially consistent making them easily validated with the manually collected data. Next, forest structural metrics are calculated at different resolutions, MLS and ALS. Second, we upscale our structural metrics to a regional extent by calibrating the metrics calculated from an ALS to those from the fine-scale MLS. From this we develop a model for ALS structural metrics and apply it over the larger G-LiHT extent for scans from 2014 and 2023. This allows us to monitor boreal forest state change and inform the development of long-term adaptive management plans for boreal regions (Figure 19). This project will support remote sensing in Forest Service monitoring programs and create a baseline for future Lidar monitoring efforts

In response to a changing climate, landscape-level monitoring has become important to develop and inform long-term adaptive management strategies such as RAD[21,27] (Figure 19). Using G-LiHT is vital for scaling up our detailed MLS findings to address landscape-level questions. Resist-Accept-Direct (RAD) is a forward-looking management approach that helps managers make informed, deliberate decisions about the trajectory of change in a forest undergoing rapid ecological transformation[9]. RAD can be used to guide boreal forests affected by climate change and disturbances to alternative stable states that are better equipped to withstand ecological contingencies[18]. Examples of management practices that would resist state changes are fire suppression and replanting existing species. These are often labor and time-intensive and do not account for ecological contingencies. Regular monitoring would allow managers to determine when a forest reaches a tipping point after which resisting is no longer sustainable. Accepting ecosystem transformation would mean not interfering with the change and allowing a new state to develop[17]. To predict future alternative stable states in boreal forests after permafrost degradation, we will use the model we created to quantify forest resilience using forest structure changes. An example of directing transformation would be anticipating the change in ecological factors and planting trees that match the emerging climate. Monitoring forest state changes is the first step to learning when and where to direct ecosystem transformation that will achieve a desired ecosystem function[18].

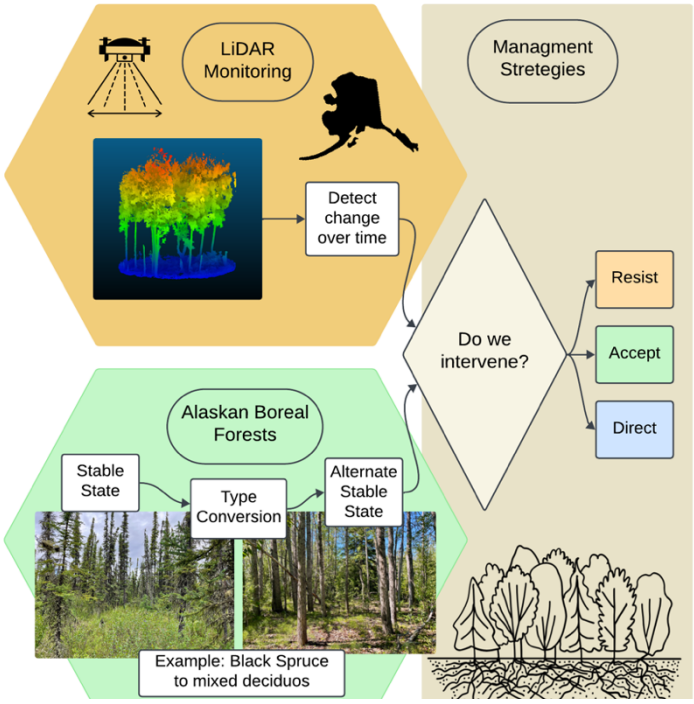

Figure 19: Conceptual Diagram of how lidar monitoring of Alaskan boreal forests informs decision-making and management strategies.

9.2 Work Cited

1. Albrich, K. et al. Simulating Forest resilience: A review. Global Ecol. Biogeogr. 29, 2082–2096 (2020).
2. Atkins, J. W. et al. Scale dependency of Lidar-derived forest structural diversity. Methods Ecol Evol 14, 708–723 (2023).

3. Bauwens, S., Bartholomeus, H., Calders, K. & Lejeune, P. Forest Inventory with Terrestrial Lidar: A Comparison of Static and Hand-Held Mobile Laser Scanning. Forests 7, 127 (2016).
4. Biskaborn, B. K. et al. Permafrost is warming at a global scale. Nat Commun 10, 264 (2019).
5. Brice, M. et al. Moderate disturbances accelerate forest transition dynamics under climate change in the temperate–boreal ecotone of eastern North America. Global Change Biology 26, 4418–4435 (2020).
6. Calvin, K. et al. IPCC, 2023: Climate Change 2023: Synthesis Report. Contribution of Working Groups I, II and III to the Sixth Assessment Report of the Intergovernmental Panel on Climate Change [Core Writing Team, H. Lee and J. Romero (Eds.)]. IPCC, Geneva, Switzerland. https://www.ipcc.ch/report/ar6/syr/ (2023) doi:10.59327/IPCC/AR6-9789291691647.
7. Camarretta, N. et al. Monitoring Forest structure to guide adaptive management of forest restoration: a review of remote sensing approaches. New Forests 51, 573–596 (2020).
8. Carpino, O. A., Berg, A. A., Quinton, W. L. & Adams, J. R. Climate change and permafrost thaw-induced boreal forest loss in northwestern Canada. Environ. Res. Lett. 13, 084018 (2018).
9. Cook, B. et al. NASA Goddard's Lidar, Hyperspectral and Thermal (G-LiHT) Airborne Imager. Remote Sensing 5, 4045–4066 (2013).
10. Davis, K. T. et al. Reduced fire severity offers near-term buffer to climate-driven declines in conifer resilience across the western United States. Proc. Natl. Acad. Sci. U.S.A. 120, e2208120120 (2023).
11. Fujii, K., Yasue, K. & Matsuura, Y. Tree ring evidence of rapid development of drunken forest induced by permafrost warming. Global Change Biology 28, 3920–3928 (2022).
12. Heidenreich, M. G. & Seidel, D. Assessing Forest Vitality and Forest Structure Using 3D Data: A Case Study From the Hainich National Park, Germany. Front. For. Glob. Change 5, 929106 (2022).
13. Hessburg, P. F. et al. Climate, Environment, and Disturbance History Govern Resilience of Western North American Forests. Front. Ecol. Evol. 7, 239 (2019).
14. Hudak, A. T. et al. A carbon monitoring system for mapping regional, annual aboveground biomass across the northwestern USA. Environ. Res. Lett. 15, 095003 (2020).
15. Hyyppä, J. et al. Unconventional LIDAR Mapping from Air, Terrestrial and Mobile.
16. Lesica, P. RAD needs monitoring. Frontiers in Ecol & Environ 20, 8–8 (2022).
17. Lynch, A. J. et al. Managing for RADical ecosystem change: applying the Resist-Accept-Direct (RAD) framework. Frontiers in Ecol & Environ 19, 461–469 (2021).
18. Magness, D. R. et al. Management Foundations for Navigating Ecological Transformation by Resisting, Accepting, or Directing Social–Ecological Change. BioScience 72, 30–44 (2022).
19. Saarinen, N. et al. Understanding 3D structural complexity of individual Scots pine trees with different management history. Ecology and Evolution 11, 2561–2572 (2021).
20. Scheffer, M., Hirota, M., Holmgren, M., Van Nes, E. H. & Chapin, F. S. Thresholds for boreal biome transitions. Proc. Natl. Acad. Sci. U.S.A. 109, 21384–21389 (2012).10
21. Schuurman, G. W. et al. Navigating Ecological Transformation: Resist–Accept–Direct as a Path to a New Resource Management Paradigm. BioScience 72, 16–29 (2022).
22. Seidel, D. A holistic approach to determine tree structural complexity based on laser scanning data and fractal analysis. Ecology and Evolution 8, 128–134 (2018).

23. Seidel, D. et al. Deriving Stand Structural Complexity from Airborne Laser Scanning Data—What Does It Tell Us about a Forest? Remote Sensing 12, 1854 (2020).
24. Seidl, R. & Turner, M. G. Post-disturbance reorganization of forest ecosystems in a changing world. Proc. Natl. Acad. Sci. U.S.A. 119, e2202190119 (2022).
25. Soja, A. J. et al. Climate-induced boreal forest change: Predictions versus current observations. Global and Planetary Change 56, 274–296 (2007).
26. Forest Resilience, Biodiversity, and Climate Change: A Synthesis of the Biodiversity / Resiliende / Stability Relationship in Forest Ecosystems. (Secretariat of the Convention on Biological Diversity, Montreal, 2009).
27. Triviño, M. et al. Enhancing Resilience of Boreal Forests Through Management Under Global Change: a Review. Curr Landscape Ecol Rep 8, 103–118 (2023).
28. Vorster, A. G., Evangelista, P. H., Stovall, A. E. L. & Ex, S. Variability and uncertainty in forest biomass estimates from the tree to landscape scale: the role of allometric equations. Carbon Balance Manage 15, 8 (2020).
29. Weldon, J. & Grandin, U. Major disturbances test resilience at a long-term boreal forest monitoring site. Ecology and Evolution 9, 4275–4288 (2019).
30. Study Sites & Design: Bonanza Creek Experimental Forest. (2002).

10 Appendix D. GitHub Repository

https://github.com/rdeinin/ALK_TLS.MLS_Processing